Article

Optimizing the Sulfates Content of Cement Using Neural Networks and Uncertainty Analysis

Dimitris C. Tsamatsoulis *, Christos A. Korologos and Dimitris V. Tsiftsoglou

Halyps Building Materials S.A., Heidelberg Materials Group, 17th Km Nat. Rd. Athens-Korinthos, 19300 Aspropyrgos, Greece; c.korologos@halyps.gr (C.A.K.); d.tsiftsoglou@halyps.gr (D.V.T.)
* Correspondence: d.tsamatsoulis@halyps.gr

Abstract: This study aims to approximate the optimum sulfate content of cement, applying maximization of compressive strength as a criterion for cement produced in industrial mills. The design includes tests on four types of cement containing up to three main components and belonging to three strength classes. We developed relationships correlating to 7- and 28-day strength with the sulfate and clinker content of the cement (CL), as well as the clinker mineral composition (tricalcium silicate, C_3S, tricalcium aluminate, C_3A). We correlated strength with the ratio $\%SO_3/CL$ and the molecular ratios MSO_3/C_3S and MSO_3/C_3A. The data processing stage proved that artificial neural networks (ANNs) fit the results' distribution better than a parabolic function, providing reliable models. The optimal $\%SO_3/CL$ value for 7- and 28-day strength was 2.85 and 3.00, respectively. Concerning the ratios of SO_3 at the mineral phases for 28-day strength, the best values were $MSO_3/C_3S = 0.132–0.135$ and $MSO_3/C_3A = 1.55$. We implemented some of the ANNs to gain a wide interval of input variables' values. Thus, the approximations of SO_3 optimum using ANNs had a relatively broad application in daily plant quality control, at least as a guide for experimental design. Finally, we investigated the impact of SO_3 uncertainty on the 28-day strength variance using the error propagation method.

Keywords: sulfates; cement; strength; clinker; optimization; artificial neural networks; model; uncertainty

1. Introduction

The most critical properties characterizing the performance of cement are early and typical compressive strength and setting time. Calcium sulfate addition affects these characteristics by simultaneously acting as a modifier and a regulator of their values [1]. The cement must contain clinker and calcium sulfate, while the standards permit the usage of other components, like limestone, pozzolans, fly ash, and slag. Gypsum is the primary source of sulfates (SO_3) composed mainly of calcium sulfate dihydrate ($CASO_4.2H_2O$ or $Cs.2H$) and a small content of anhydrite ($CaSO_4$ or Cs). During cement grinding, elevated temperatures partially dehydrate gypsum into hemihydrate form or bassanite ($CaSO_4.0.5H_2O$ or $Cs.0.5H$) [2]. Copeland et al. [3] and a recent systematic review [4] clarify the solubility of the three phases of $CaSO_4$.

Clinker is mainly composed of four mineral phases: tricalcium silicate ($3CaO \cdot SiO_2$ or C_3S), dicalcium silicate ($2CaO \cdot SiO_2$ or C_2S), tricalcium aluminate ($3CaO \cdot Al_2O_3$ or C_3A), and tetra calcium aluminoferrite ($4CaO \cdot Al_2O_3 \cdot Fe_2O_3$ or C_4AF). Bogue established the mathematical formulae for calculating the four clinker compounds as a function of the percentages of the four basic oxides CaO, SiO_2, Al_2O_3, Fe_2O_3, or C, S, A, F, as well as the free lime CaO_f [5] (pp. 245–250).
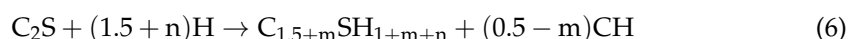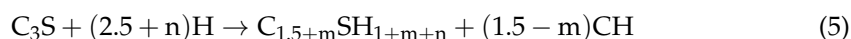
$$C_3S = 4.07 \times (CaO - CaO_f) - 7.6 \times SiO_2 - 6.72 \times Al_2O_3 - 1.43 \times Fe_2O_3 \qquad (1)$$

$$C_2S = 2.87 \times SiO_2 - 0.754 \times C_3S \qquad (2)$$

$$C_3A = 2.65 \times Al_2O_3 - 1.69 \times Fe_2O_3 \qquad (3)$$

$$C_4AF = 3.04 \times Fe_2O_3 \qquad (4)$$

The reactions of these four mineral components with water (H) give rise to various compounds, in which the dominant phases are calcium silicate hydrates (C-S-H) and calcium hydroxide (CH). Equations (5) and (6) express generalized forms of the hydration reactions of C_3S and C_2S, including some small decimal numbers m and n [1].

$$C_3S + (2.5 + n)H \rightarrow C_{1.5+m}SH_{1+m+n} + (1.5 - m)CH \qquad (5)$$

$$C_2S + (1.5 + n)H \rightarrow C_{1.5+m}SH_{1+m+n} + (0.5 - m)CH \qquad (6)$$

Gypsum addition also obstructs the fast exothermic reaction of C_3A by forming ettringite ($C_3A.3Cs.32H$), according to Equation (7).

$$C_3A + 3Cs + 32H \rightarrow C_3A.3Cs.32H \qquad (7)$$
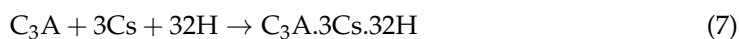
Ettringite formation regulates uncontrolled C_3A hydration, preventing flash set during concrete production, transfer, and placement [6–8]. Conversely, adding too much gypsum leads to a drop in strength and detrimental expansion of concrete and mortar, meaning there is a sulfate optimum. Cement standards, such as EN 197-1:2011 [9] and ASTM C150 [10], prohibit sulfates above a certain level per type of cement, though they do not suggest an optimal value because that figure depends on the various physical, chemical, and mechanical properties of cement and clinker produced in the specific conditions of each production unit. Furthermore, the property to be optimized impacts the location of the optimum. Some standards, such as ASTM C563-16 [11], define a method for determining the optimal SO_3, albeit only for a particular property of cement, i.e., 1-day compressive strength.

Historically, determining the optimal sulfates in cement was subjected to intensive and continuous research. In recent years, a primary goal of the cement industry was the reduction in its carbon footprint by decreasing CO_2 emissions in clinker production and clinker consumption per ton of product. Optimizing the composition of raw materials for clinker production can achieve the above goal [12,13]. Optimizing SO_3 is essential for reducing clinker incorporation into the cement while retaining or improving product performance. Lerch [14] conducted the first thorough study of sulfate optimization in cement past and mortar. According to the researcher, the optimal sulfate content in cement is closely related to hydration heat, length changes of mortar specimens cured in water, alkalis, C_3A content, and cement fineness. Fincan [15] mentions that Lerch was a pioneer and inspired many studies on sulfate optimization in cement and cementitious systems.

Several researchers investigated the impact of SO_3 on the hydration of the clinker mineral phases [16–25]. Bentur [16] found that gypsum influenced the quantity and quality of the hydrated products by accelerating the hydration process and, at the same time, lowering the intrinsic strength of the gel. He interpreted the effect of gypsum on strength in terms of its influence on the extent of hydration and the chemical composition of the gel. Soroka et al. [18] concluded that gypsum accelerates the rate of hydration when its addition is below the optimum SO_3 content. Nevertheless, if the gypsum added exceeds the optimal level, considerable obstruction occurs. The authors did not observe any effect of the SO_3 content on the density of the hydration products and pore-size distribution. They pointed out that further study is required to explain the impact of SO_3 on strength. On the contrary, Sersale et al. [19] found that gypsum addition modified the microstructure of Portland cement mortars. They correlated these modifications with the mechanical behavior of cement mortars by examining Portland cement with sulfate content ranging between 1.5 and 4.5%. A SO_3 content of 2–3.5% promotes a shifting in the pore size distribution to lower values, ranging between 100 and 1000 Å, and a variation in total porosity. They concluded

that this issue is likely the main factor governing the influence of SO_3 on the compressive strength of Portland cement. Gunay [22], in his thesis, studied the influence of aluminates hydration in the presence of calcium sulfate on C_3S hydration and its consequences on cement optimum sulfate. He observed the SO_3 optimum when the hydration of C_3S, during the accelerated period, takes place simultaneously or slightly before the exothermic peak due to the dissolution of C_3A and the precipitation of mono-substituted Al_2O_3 and Fe_2O_3 (AFm). He concluded that the presence of AFm during the accelerated period of C_3S hydration would be the cause of the observed modification of the microstructure of the cement paste: the porosity increases with the addition of calcium sulfate, though the assembly of hydrates is denser. This effect of the sulfate level is the source of the optimal compressive strength observed by Gunay. Zunino et al. [24] investigated the influence of sulfate addition on hydration kinetics and the C-S-H morphology of C_3S and C_3S/C_3A systems at an early age. Adding gypsum changed the needle length of C-S-H and increased the nucleation density. In C_3S/C_3A systems, they did not observe any difference in C-S-H morphology before and after the aluminate peak. Andrade Neto et al. [25] studied the hydration and interactions between pure and doped C_3S and C_3A in the presence of different calcium sulfates. Except for sulfates of gypsum, Miller et al. [26], Taylor [27], and Horkoss et al. [28] investigated the importance of the amount and phases of SO_3 incorporated into the clinker. Mohammed et al. [29] optimized the SO_3 content of a CEM I cement via grinding clinker with a ball mill until a fineness of 3270 cm^2/g was achieved, before preparing mixes with ground gypsum ranging from 0 to 9%. According to their results, the water demanded for normal consistency, setting times, compressive strength, the heat of hydration, swelling, drying shrinkage, and hydration degree are adversely affected by gypsum addition above or below the optimal. For this cement, which was composed only of clinker and gypsum, they found that the optimal sulfate for 2-, 7-, and 28-day strength was 3%.

Nowadays, with the reduction in CO_2 emissions being imperative, composite types of cement constitute the bulk of the products of the cement industry, rendering the optimization of sulfates in such cement more relevant. During the last few decades, numerous researchers conducted deep research investigating the optimal sulfate content of cement containing supplementary cementitious materials (SCM) [30–36]. Yamashita et al. [30] investigated the influence of limestone powder (LSP) on the optimum SO_3 for Portland cement samples with different Al_2O_3 contents, which was not negligible. Analyses showed that if SO_3 is less than optimal, an increase in sulfate promotes hydration in C_3A and increases compressive strength. In the presence of higher SO_3 content, excess formation of expansive ettringite introduced more pores, and compressive strength decreased. After adding LSP, a lower sulfate content was adequate to obtain the maximum compressive strength. Liu et al. [32] examined the effect of gypsum content on cementitious mixtures containing limestone, fly ash, and slag by studying several properties: initial and final setting time, past fluidity, water demand, and strength. Adu-Amankwah et al. [33] conducted detailed research into the consequence of sulfate additions on hydration and the performance of ternary slag–limestone composite cement using complementary techniques. Their results showed that the presence of sulfate influenced the early-age reaction kinetics of the clinker phases and supplementary cementitious materials. These changes impacted the total porosity and cement strength in opposing ways: porosity was reduced with increasing ettringite fraction, while the lower water content of the C-S-H reduced the space-filling capacity of the C-S-H. Han et al. [34] investigated the effect of gypsum on the properties of composite binders containing high-volume slag and iron tailing powder using multiple measuring techniques. They concluded that although incorporating gypsum promoted early hydration of cement and slag, it limited their further hydration at later ages. Added gypsum formed a large amount of ettringite and densified early-age pore structure, though it coarsened later-age pore structure. Fiscan [15] optimized sulfate in cement–slag blends based on calorimetry and early strength results, investigating the influence of fineness, C_3A, C_4AF of cement, and the Al_2O_3 content of slag on the optimum SO_3. Niemuth [7]

examined the effect of fly ash on the optimum sulfate content in Portland cement, providing experimental data on strength development and heat release during early hydration for cement–fly ash systems with different SO_3 levels. He demonstrated that some fly ash samples achieve their sulfate demand. When a cement contains these samples, there is effectively an increase in the optimal SO_3 level compared to the corresponding CEM I Portland cement. In his research into the optimal SO_3 content of Portland and pozzolanic cement types, Tsamatsoulis et al. [35] reached the same conclusion.

Increasingly, cement manufacturers use grinding aids/strength improvers to reduce energy consumption and improve cement quality. According to Magistri et al. [37], hydration in the presence of such additives proceeds differently than in cement produced without them, remarkably improving cement properties. Hirsch et al. [38] examined the impact of triethanolamine (TEA) on the sulfate balance of Portland cement with mixed sulfate carriers (Cs.2H, Cs.0.5H, CS). Their results indicated that TEA influenced the balance of sulfate and aluminate-containing clinker phases. These effects were closely related to the types and amounts of the sulfate carriers present in the cement. The very practical, from a process point of view, research of Recchi et al. [39] investigates the influences of the type (Cs.2H, Cs.0.5H, Cs) and amount of calcium sulfate on the reactivity of TEA and tri-isopropanolamine (TIPA) strength improvers, which are today's most widely used alkanolamines. TEA is an early compressive strength enhancer, while TIPA increases the late strengths. The authors concluded that if the sulfate carrier is bassanite, the early strength increase obtained with the addition of TEA is more evident due to the higher solubility of Cs.0.5H. On the other hand, TIPA is significantly less efficient at increasing late strength when bassanite is the source of SO_3, i.e., Cs.0.5H is not preferable when the objective of TIPA use is to enhance 28-day strength. Andrade Neto et al. [40] recently conducted a detailed review of the effect of SO_3 on cement hydration, noticing that despite many years of research, questions regarding sulfate optimization remain. Further investigation into the influence of clinker and $CaSO_4$ characteristics using different supplementary cementitious materials and chemical admixtures is needed.

Some researchers provided or applied equations correlating optimal SO_3 with the cement's chemical and physical characteristics. For achieving maximum 28-day strength with C_3A, K_2O, Na_2O, and fineness of cement, Schade et al. [41] presented three equations (Haskell, Jawed and Skalny, and Ost). They utilized the third equation to perform a design of experiments (DoE) to model the sulfate amounts in ultra-finely ground and fast-hardening clinker. Kurdowski [42] reported four equations for approximating the optimal SO_3 content (Ost, Lerch, Jirku, and Haskell), before noticing that these empirical equations have limited accuracy, even if they include the main factors affecting the optimum gypsum addition. He considered that using experimentation to determine the most convenient sulfate addition is the best approach. Andrade Neto et al. [40] summarized the laboratory methods for determining the correct SO_3 content in conjunction with their advantages and disadvantages. From an industrial perspective, strength measurement is the most utilized method, since compressive strength is a key performance criterion for producers and customers. ASTM C563-16 [11] describes the determination of approximate optimum SO_3 for maximum compressive strength by measuring the change in this property of cement mortar as a result of substituting calcium sulfate for a portion of the cement. The standard suggests a parabolic equation between strength and sulfate that optimally fits the experimental points when assuming a symmetric distribution. The optimal SO_3 approximation corresponds to the value providing the vertex of the parabola. The standard clearly states that in cases of a skewed function of the strength versus sulfate to the right or left of the peak, an asymmetric distribution function may provide a better fit. Niemuth [7], Tsamatsoulis [35], and Fincan [15] applied the parabolic formula in their attempts to find an adequate approximation of SO_3 optimal content. Tsamatsoulis [35], when trying to determine a unified function for several cement types with variable clinker content, used the ratio of sulfate amount to clinker percent (%SO_3/CL) as an independent variable.

This study aims to approximate the optimal SO_3 content of cement using the maximization of compressive strength as a criterion for cement produced in industrial mills. The experimental design includes tests on four types of cement containing up to three main components, except gypsum, and belonging to three strength classes. We developed several relationships correlating the 7- and 28-day strengths of the sulfate and clinker content of the cement and the clinker mineral composition. We normalized the results to obtain unique functions for all experimental data, using an approach similar to the method presented in [35]. This study proved that a shallow artificial neural network [43,44] fits the data distribution better than a parabolic function. Finally, we focused on the impact of SO_3 uncertainty on the 28-day strength variance using the error propagation method. The structure of the paper is as follows: Section 2 includes the sampling procedure, experimental methods, and test results; Section 3 describes the implemented algorithms for data processing, including a detailed discussion of each set of results; and, finally, Section 4 summarizes the main conclusions of this research.

2. Materials and Methods

In this study, we chose to optimize the sulfate amount of the basic cement types produced according to EN 197: 2011 [9] in the Halyps cement plant, using the compressive strength criterion as a guide. Table 1 shows the CEM types investigated and the norm requirements as regards composition and strength limits. The nominal composition did not contain the gypsum. The producer was responsible for adjusting its content by respecting the maximum SO_3 limit, which was 4% for CEM I 52.5 N and 3.5% for the other three CEM types. We observed that the research covered a wide range of Portland (CEM I, CEM II) and pozzolanic (CEM IV) types. The study was, therefore, general for the cement products of this specific cement plant. The optimal value of cement sulfate depended on various factors, which were summarized by Andrade Neto et al. [40] as follows: (a) clinker mineralogy (C_3S, C_3A) and alkali content, as well as cement and clinker fineness; (b) form of SO_3 carriers (Cs.2H, Cs.0.5H, Cs or alkali sulfates), as well as mineral or chemical gypsum; (c) intergrinding or separate grinding of clinker and gypsum; (d) content and type of SCM; (e) grinding aid/strength improver type; (f) hydration age; (g) water/binder ratio; and (h) curing conditions. Using the standard EN 196-1 [45] to create mortars, we attempted to find the SO_3 contents for maximum 7- and 28-day strength and examined the optimum position as a function of hydration age, fulfilling the conditions (f)–(h).

Table 1. CEM types tested.

CEM	Constituent (%)				28-Day Strength Limits (MPa)	
	Clinker	Limestone	Pozzolan	Minor	Low	High
CEM I 52.5 N	95–100			0–5	52.5	
CEM II A-L 42.5 N	80–94	6–20		0–5	42.5	62.5
CEM II B-M (P-L) 32.5 N	65–79	21–35		0–5	32.5	52.5
CEM IV B(P) 32.5 N-SR	45–64		36–55	0–5	32.5	52.5

The goal of the experimentation was to obtain cement samples as close as possible to industrially produced cement in terms of fineness, chemical characteristics, forms of the sulfate carriers, and interaction of the grinding aid with the solids. Grinding in the Halyps cement plant was performed through co-grinding the raw materials in closed-circuit mills equipped with high-performance separators and co-feeding a 28-day strength enhancer into the mill feed. In an earlier study [46], we found that for a step change in gypsum, the mill circuit required around 1 h to reach the steady state regarding SO_3. For each CEM type, by operating the mill in automatic mode and after stabilizing the circuit around the operating set points and the desired fineness, we suddenly decreased the gypsum to 2%. There was no change in the percentage of clinker, while another material increased in proportion (limestone or pozzolan). Sampling of around 20 kg of the final product followed

after 1.5 h. The second step was an increase in gypsum to 7.5% and a proportional decrease in limestone or pozzolan to maintain the %clinker constant. Further sampling took place 1.5 h after this change. During this process, with an operation kept as constant as possible, the laboratory sampled clinker at the mill inlet. In this way, the lab created two samples of industrial cement with low and high gypsum for each CEM type. Mixing them in proper proportions yielded samples with suitable SO_3 values usable to correlate strength and sulfate. The industrial tests of the four CEM types were realized within two months to allow the clinker composition to incorporate the actual production variances.

The samples' analysis comprised several mechanical, physical, and chemical tests: (i) fineness with air-jet sieving and specific surface with Blaine apparatus, using EN 196-6 [47]; (ii) loss on ignition (LOI), insoluble residue (InsRes), and oxides analysis via XRF by applying EN 196-2 [48]; (iii) laser particle size analysis; (iv) compressive strength measurement using EN 196-1; and (v) clinker and cement phases using XRD. Halyps lab conducted the analyses (i)–(iv), while the Devnya Cement lab performed the XRD analysis.

2.1. Clinker and Raw Materials Analysis

Aside from the experiment illustration, clinker, gypsum, limestone, and pozzolan analyses used during the test are necessary for estimating the CEM composition. Table 2 demonstrates the XRF and XRD analyses of the four clinkers. The mean values of the loss on ignition and insoluble residue were equal to 0.3. Equation (8) presents the molecular ratio between SO_3 and alkalies, i.e., MSO_3.

$$MSO_3 = \frac{SO_3}{80} \bigg/ \left(\frac{K_2O}{94} + \frac{Na_2O}{62} \right) \tag{8}$$

Table 2. Clinker XRF and XRD analyses.

	XRF Analysis (%)									Phases According to Bogue				
Clinker for CEM	SiO$_2$	Al$_2$O$_3$	Fe$_2$O$_3$	CaO	MgO	SO$_3$	K$_2$O	Na$_2$O	CaO$_f$	C$_3$S	C$_2$S	C$_3$A	C$_4$AF	MSO$_3$
I 52.5 N	21.05	4.83	3.08	66.08	1.86	1.04	0.78	0.41	1.58	65.7	10.9	7.6	9.4	0.87
II A-L 42.5 N	20.95	5.13	3.14	66.59	1.60	0.81	0.72	0.27	1.24	67.8	9.0	8.3	9.5	0.84
II B-M (P-L) 32.5 N	21.06	5.45	3.08	66.46	1.48	0.70	0.66	0.31	1.52	63.2	12.8	9.2	9.4	0.73
IV B (P) 32.5 N	21.08	4.78	2.98	66.15	2.12	0.97	0.78	0.34	2.56	62.2	13.6	7.6	9.1	0.88
Mean value						0.88				64.7				0.83
Std. Dev.						0.15				2.5				0.07

	XRD Analysis							
Clinker for CEM	M$_3$ C$_3$S	M$_1$ C$_3$S	Total C$_3$S	C$_2$S	C$_4$AF	C$_3$A Cubic	C$_3$A Ortho	Total C$_3$A
I 52.5 N	23.3	37.9	61.2	20.7	8.2	2.8	3.7	6.5
II A-L 42.5 N	29.8	37.1	66.9	15.4	8.8	2.8	3.7	6.5
II B-M (P-L) 32.5 N	25.2	40.2	65.4	16.9	8.5	2.5	4.2	6.7
IV B (P) 32.5 N	25.1	35.7	60.8	21.2	7.9	2.6	4.0	6.6

	K$_2$SO$_4$	Na$_2$SO$_4$	K$_2$SO$_4$.2CaSO$_4$	3K$_2$SO$_4$.Na$_2$SO$_4$	CaSO$_4$
Clinker for CEM	Arcanite	Thenardite	Langbeinite	Aphthitalite	Anhydrite
I 52.5 N	0.28	0	0	0.52	0
II A-L 42.5 N	0.44	0	0	0.58	0
II B-M (P-L) 32.5 N	0.36	0	0	0.58	0
IV B (P) 32.5 N	0.21	0	0	0.73	0

Table 2 presents the mean values and standard deviations of SO_3, C_3S, and MSO_3. The corresponding annual values for 2022 of the Halyps clinker were as follows: $SO_3 = 0.86 \pm 0.25$, $C_3S = 64.7 \pm 2.5$, and $MSO_3 = 0.88 \pm 0.24$; these results mean that the variance in the four clinkers' properties covers a significant amount of the actual variability in the plant clinker in terms of quality. The mineral phases measured via XRD differ from those computed with Bogue formulae, though the C_3S values fit relatively well. XRD did not detect anhydrite

and langbeinite because the $MSO_3 < 1$. Table 3 presents the average analysis of the three raw materials. Assuming that CaO, MgO, SO_3, and LOI exist in gypsum in the form of calcium and magnesium carbonates, gypsum dihydrate, and anhydrite, we computed these four components by solving the corresponding linear system. The results show that gypsum is mainly dihydrate, containing a small percentage of anhydrite.

Table 3. Raw materials analyses.

Materials	SiO$_2$	Al$_2$O$_3$	Fe$_2$O$_3$	CaO	MgO	SO$_3$	K$_2$O	Na$_2$O	LOI (%)	InsRes (%)
					XRF Analysis (%)					
Gypsum	1.26	0.81	0.17	31.31	1.60	43.29	0.14	0.01	20.95	0
Limestone	1.08	0.33	0.06	54.22	1.39	0.02	0.10	0.03	42.82	0
Pozzolan	73.61	12.24	1.90	0.87	0.19	0	3.61	3.90	2.84	90.5

Gypsum	CaSO$_4$.2H$_2$O	CaSO$_4$	CaCO$_3$	MgCO$_3$
Compounds (%)	87.9	4.1	1.8	3.4

2.2. Cement Analyses

The laboratories conducted chemical, physical, and mechanical tests on the cement samples to reliably correlate the variables and minimize uncertainties. Table 4 provides both the chemical analysis of the eight samples taken for the CEM types under investigation and the gypsum phases within the cement measured via XRD. We also took advantage of the automatic recording of process data in the plant database to find the cement temperature at the mill outlet for each of the eight tests. Table 4 shows the mean value of this temperature (T_{CEM}) for each of the eight tests. Although the detection of gypsum phases via XRD could be approximated, the main conclusion was that hemihydrate was null or negligible. This issue arose because the cement temperature at the mill outlet never reached 100 °C, as dihydrate starts to dehydrate to Cs.0.5H [49]. Krause et al. [50] experimentally found that the transformation of gypsum into hemihydrate could take place at a temperature of 50 °C. However, our industrial results do not verify these findings.

Table 4. Chemical analysis of cement samples.

CEM Type	Gypsum (%)	SiO$_2$	Al$_2$O$_3$	Fe$_2$O$_3$	CaO	MgO	SO$_3$	K$_2$O	Na$_2$O	LOI (%)	InsRes (%)
						XRF Analysis (%)					
I 52.5 N	2	18.98	4.55	2.82	63.89	1.78	2.14	0.65	0.33	4.08	0.25
I 52.5 N	7.5	19.00	4.55	2.83	62.90	1.79	4.19	0.63	0.34	3.00	0.28
II A-L 42.5 N	2	16.82	3.85	2.30	63.12	1.47	1.42	0.67	0.22	9.58	0.29
II A-L 42.5 N	7.5	16.68	3.89	2.30	62.23	1.49	3.59	0.60	0.23	8.43	0.24
II B-M (P-L) 32.5 N	2	19.78	4.26	2.08	58.09	1.30	1.27	0.80	0.47	11.44	6.74
II B-M (P-L) 32.5 N	7.5	19.64	4.19	2.08	56.83	1.30	3.52	0.81	0.58	10.53	6.68
IV B (P) 32.5 N	2	38.75	6.87	2.49	41.23	1.44	1.55	1.87	1.49	3.54	30.78
IV B (P) 32.5 N	7.5	35.16	6.33	2.43	43.54	1.52	3.26	1.67	1.29	4.06	32.37

CEM Type	Gypsum (%)	CaSO$_4$.2H$_2$O	CaSO$_4$.0.5H$_2$O	CaSO$_4$	T$_{CEM}$ (°C)
			Gypsum phases (%)		
I 52.5 N	2	1.52	0.01	0.21	80.3
I 52.5 N	7.5	4.39	0.1	0.8	82.2
II A-L 42.5 N	2	1.56	0	0.23	67.0
II A-L 42.5 N	7.5	5.15	0	1	74.6
II B-M (P-L) 32.5 N	2	1.61	0	0	66.3
II B-M (P-L) 32.5 N	7.5	4.31	0.05	0.55	77.1
IV B (P) 32.5 N	2	1.8	0	0.26	70.6
IV B (P) 32.5 N	7.5	5.5	0	0.69	75.7

Table 5 shows the fineness measurements of these samples expressed as %residues in 40, 32, and 20 microns (R40, R32, R20) and obtained via air-jet sieving and Blaine. All samples had 100% passing in the 90 microns sieve (R90 = 0). The same table demonstrates

several fineness modules obtained via laser particle size analysis: diameters of 50%, 90%, and 10% passing (D50, D90, D10), as well as percentages between 32 and 3 microns (P32–R3).

Table 5. Fineness of cement samples.

CEM Type	Gypsum (%)	R40 (%)	R32 (%)	R20 (%)	Blaine (cm²/g)	D50 (μ)	D90 (μ)	D10 (μ)	P32-R3 (%)
I 52.5 N	2	7.5	10.2	33.6	3350	13.5	39.3	1.5	63.4
I 52.5 N	7.5	6.5	7.0	28.7	3520	12.3	34.5	1.4	66.9
II A-L 42.5 N	2	5.5	6.7	28.5	3830	11.0	34.1	1.3	65.0
II A-L 42.5 N	7.5	6.1	6.9	27	4010	10.7	33.4	1.1	65.1
II B-M (P-L) 32.5 N	2	8.1	10.7	33.2	3920	11.5	38.1	1.3	61.6
II B-M (P-L) 32.5 N	7.5	6.8	8.8	30.8	3980	11.0	35.8	1.1	62.8
IV B (P) 32.5 N	2	8.5	17.4	39.5	3450	15.3	45.7	1.5	59.4
IV B (P) 32.5 N	7.5	8	16.2	38	3570	13.6	41.6	1.3	60.8

The solution of a linear system, as given in Equations (9)–(12) and expressing the mass balances, provided the dry cement composition of all samples using chemical analysis of cement, clinker, and raw materials. This estimation avoided the uncertainties of the mill feeders where the raw materials had a certain percentage of moisture.

$$CL + G + Lim + Pz = 100 \tag{9}$$

$$SO_{3\,CL}\frac{CL}{100} + SO_{3\,G}\frac{G}{100} + SO_{3\,Lim}\frac{Lim}{100} + SO_{3\,Pz}\frac{Pz}{100} = SO_{3\,CEM} \tag{10}$$

$$LOI_{CL}\frac{CL}{100} + LOI_G\frac{G}{100} + LOI_{Lim}\frac{Lim}{100} + LOI_{Pz}\frac{Pz}{100} = LOI_{CEM} \tag{11}$$

$$InsRes_{CL}\frac{CL}{100} + InsRes_G\frac{G}{100} + InsRes_{Lim}\frac{Lim}{100} + InsRes_{Pz}\frac{Pz}{100} = InsRes_{CEM} \tag{12}$$

CL, G, Lim, and Pz are the clinker, gypsum, limestone, and pozzolan percentages With $SO_{3\,X}$, LOI_X, and $InsRes_X$, we denoted the sulfate, loss on ignition, and insoluble residue of the material X (X = CL, G, Lim, Pz, CEM). Solving the system of (9)–(11) produced the composition of CEM I 52.5 N and CEM II A-L 42.5 N. The calculation of the Pz requires the solution of the system (9)–(12) for CEM II B-M(P-L) 32.5 N. For the CEM IV(P) 32.5 N with high pozzolan content, our algorithm used three additional equations that expressed the mass balances of SiO_2, Al_2O_3, and CaO. The composition results from the error minimization between the actual and calculated chemical analysis of cement were realized using the Generalized Reduced Gradient non-linear regression method. The lab conducted a chemical analysis, except for the eight samples, of the residues at 40, 32, and 20 microns of each of them. By determining the composition of the total sample and the material retained in each sieve, we calculated the %constituents of the material that passes through that sieve. The above approach made it feasible to calculate the composition in each fraction and investigate the grindability of the materials during co-grinding. Table 6 depicts the %components of the samples and passings through the three mentioned sieves and the residues of each material in the three sieves. Equations (13) and (14) provide these values.

$$CompPass_{k,j} = \frac{CompSample_k - \frac{R_j}{100}\cdot CompRes_{k,j}}{1 - \frac{R_j}{100}} \quad k = 1\ to\ 4,\ j = 1\ to\ 3 \tag{13}$$

$$RM_{k,j} = 100\cdot\left(1 - \frac{CompSample_k - \frac{R_j}{100}\cdot CompRes_{k,j}}{CompSample_k}\right) \quad k = 1\ to\ 4,\ j = 1\ to\ 3 \tag{14}$$

Table 6. Compositions of cement samples and passing in each sieve and materials' residues.

	Gypsum (%)	Compositions of Samples and Passings				Gypsum (%)	Compositions of Samples and Passings			
CEM Type	Sieve	CL [1] (%)	G [2] (%)	Lim [3] (%)	Pz [4] (%)	Sieve	CL (%)	G (%)	Lim (%)	Pz (%)
I 52.5 N	2, sample	89.7	2.8	7.5	0	7.5, sample	89.8	7.5	2.7	0
	2, 40 µ	89.1	3.0	7.9	0	7.5, 40 µ	89.3	7.9	2.8	0
	2, 32 µ	88.9	3.1	8.1	0	7.5, 32 µ	89.3	7.9	2.8	0
	2, 20 µ	86.3	4.0	9.8	0	7.5, 20 µ	86.9	9.7	3.4	0
II A-L 42.5 N	2, sample	77.2	1.8	21.0	0	7.5, sample	77.4	6.8	15.8	0
	2, 40 µ	76.4	1.9	21.7	0	7.5, 40 µ	76.3	7.2	16.6	0
	2, 32 µ	76.1	2.0	21.9	0	7.5, 32 µ	76.2	7.2	16.6	0
	2, 20 µ	71.2	2.5	26.4	0	7.5, 20 µ	71.8	8.7	19.5	0
II B-M (P-L) 32.5 N	2, sample	66.0	1.9	24.9	7.2	7.5, sample	65.6	7.1	20.2	7.2
	2, 40 µ	64.9	2.0	26.3	6.8	7.5, 40 µ	64.7	7.4	21.2	6.7
	2, 32 µ	64.3	2.0	26.8	6.8	7.5, 32 µ	64.3	7.5	21.6	6.7
	2, 20 µ	57.7	2.6	32.5	7.2	7.5, 20 µ	59.1	8.9	25.9	6.2
IV B (P) 32.5 N	2, sample	59.2	2.3	4.3	34.2	7.5, sample	57.2	6.4	3.6	32.9
	2, 40 µ	59.7	2.5	4.6	33.2	7.5, 40 µ	57.1	6.8	3.8	32.3
	2, 32 µ	60.3	2.7	5.0	32.0	7.5, 32 µ	56.9	7.3	4.1	31.7
	2, 20 µ	59.1	3.3	6.0	31.5	7.5, 20 µ	53.9	8.8	4.8	32.5
	Gypsum (%)	Residues (%)				Gypsum (%)	Residues (%)			
	Sieve	CL	G	Lim	Pz	Sieve	CL	G	Lim	Pz
I 52.5 N	2, 40 µ	8.1	1.1	2.6		7.5, 40 µ	7.0	1.7	2.4	
	2, 32 µ	11.0	1.6	3.8		7.5, 32 µ	7.6	1.9	2.5	
	2, 20 µ	36.1	5.7	13.5		7.5, 20 µ	31.0	7.6	10.8	
II A-L 42.5 N	2, 40 µ	6.6	0.5	2.0		7.5, 40 µ	7.4	1.7	1.6	
	2, 32 µ	8.0	0.6	2.3		7.5, 32 µ	8.3	1.9	2.2	
	2, 20 µ	34.1	2.6	10.1		7.5, 20 µ	32.3	7.1	10.0	
II B-M (P-L) 32.5 N	2, 40 µ	9.7	1.8	2.9	13.0	7.5, 40 µ	8.1	2.4	2.3	12.3
	2, 32 µ	13.0	2.3	3.9	15.7	7.5, 32 µ	10.6	3.0	2.7	15.0
	2, 20 µ	41.6	6.6	12.7	33.8	7.5, 20 µ	37.6	13.2	11.3	40.5
IV B (P) 32.5 N	2, 40 µ	7.6	1.4	1.5	11.3	7.5, 40 µ	8.1	1.9	2.1	9.7
	2, 32 µ	15.8	2.8	3.3	22.9	7.5, 32 µ	16.6	3.8	4.9	19.2
	2, 20 µ	39.5	12.1	15.6	44.3	7.5, 20 µ	41.6	14.2	16.8	38.7

[1] CL = Clinker, [2] G = Gypsum, [3] Lim = Limestone, [4] Pz = Pozzolan.

The j indexes from 1 to 3 correspond to the sieves at 40, 32, and 20 microns, while the k indexes 1 to 4 correspond to the four materials (clinker, gypsum, limestone, pozzolan). R_j is the residue of a sample at the sieve j, and $RM_{k,j}$ is the residue of material k at the sieve j. $CompSample_k$ is the percentage of the component k within the sample, while $CompRes_{k,j}$ and $CompPass_{k,j}$ are the percentages of the component k in the residue and passing in the sieve j.

These results indicate the higher grindability of gypsum and limestone compared to the other compounds. We observed that clinker and pozzolan had similar grindability. Therefore, approximating the optimal SO_3 content using industrially produced cement in a closed-circuit mill was crucial. It was difficult to obtain the same particle size per constituent and the distribution of the grinding aid via grinding in an open circuit lab apparatus or interblending the previously ground materials. Tang et al. [51] concluded that when testing to determine the optimum sulfate content, it was significant to co-grind the calcium sulfate with clinker because co-grinding resulted in lower sulfate demand than interblending. Thus, the results obtained via the latter method would not be representative.

2.3. Cement Samples Mixing and Related Tests

The lab mixed the cement samples of low and high gypsum to create new samples at regular and proper intervals of SO_3 values. Complete chemical analysis of these samples, composition calculation—as described in Section 2.2—mortars preparation, and measuring the 7- and 28-day compressive strengths followed.

Table 7 depicts the proportions of low and high gypsum samples, the SO_3 and %Clinker values, the %ratio of sulfates to clinker (%SO_3/CL), and the 7- and 28-day compressive

strengths of each mix for the four CEM types investigated. SO_3 values stem from XRF measurement, while %Clinker results stem from composition calculation.

Table 7. Cement analysis and compressive strength.

	Sample with Gypsum					Compressive Strength	
CEM Type	Low (%)	High (%)	SO$_3$ (%)	Clinker (%)	%SO$_3$/CL	7-Day (MPa)	28-Day (MPa)
I 52.5 N	100	0	2.14	89.7	2.39	47.2	60.8
	80	20	2.46	89.8	2.74	45.6	62.1
	70	30	2.67	89.4	2.99	46.4	63.2
	60	40	2.87	89.7	3.20	48.6	61.5
	50	50	3.09	89.5	3.45	44.5	61.8
	40	60	3.30	89.7	3.68	45.5	61.4
	30	70	3.51	89.9	3.90	46.9	63.5
	20	80	3.70	89.5	4.13	43.9	57.6
II A-L 42.5 N	100	0	1.42	77.2	1.84	41.4	51.6
	80	20	1.87	77.5	2.41	44.2	53.6
	60	40	2.28	77.5	2.94	45.6	54.0
	60	40	2.29	77.5	2.95	44.3	53.4
	50	50	2.49	77.6	3.21	44.5	52.3
	40	60	2.71	77.5	3.50	44.0	52.3
	30	70	2.98	77.3	3.86	43.3	52.6
	20	80	3.15	77.5	4.07	42.7	50.5
	20	80	3.17	77.5	4.09	40.7	51.3
	0	100	3.59	77.4	4.64	40.0	49.2
II B-M (P-L) 32.5 N	100	0	1.27	66.0	1.92	34.2	43.5
	80	20	1.74	66.2	2.63	36.3	44.4
	65	35	2.08	65.2	3.19	34.1	45.0
	60	40	2.21	66.1	3.34	35.1	45.3
	50	50	2.43	66.0	3.68	34.5	44.7
	40	60	2.67	65.8	4.06	32.3	41.2
	40	60	2.64	66.2	3.99	32.7	41.2
	20	80	3.09	65.7	4.70	29.8	40.4
	0	100	3.52	65.6	5.37	27.2	38.0
IV B (P) 32.5 N	85	15	1.77	57.4	3.08	24.9	37
	80	20	1.84	57.3	3.21	23.5	36.9
	68	32	2.04	58.3	3.50	23	35.9
	55	45	2.28	58.2	3.92	23.1	34.1
	40	60	2.53	58.9	4.30	21.8	33.9
	20	80	2.88	58.9	4.89	20.7	33.5

In Appendix A, we provide a list of raw materials suppliers and the manufacturers of the main equipment used.

3. Data Processing and Results

3.1. Correlation of Strength with Sulfates and Clinker Content

The results of Table 7 indicate that the 7- and 28-day strengths depend strongly on the %Clinker and SO_3 values. Cement fineness, the clinker's mineral composition, supplementary cementitious materials, and the kind and dosage of strength enhancer also impact compressive strength. The results shown in Table 5 show that the fineness at 40 microns was similar for samples of 2 and 7.5% gypsum for each CEM type. Therefore, the same method would apply to the prepared mixes. Furthermore, we used the same type and dosage of strength improver for all CEM types, which enhances the 28-day strength. As the SO_3 value used to obtain maximum strength depends on the clinker content, we used the ratio %SO_3/CL–SO_3/CL as an independent variable. Our algorithm used the following dimensionless 7- and 28-day strengths to normalize the results for all CEM types.

$$RelStr7 = \frac{Str7}{MaxStr7} \tag{15}$$

$$RelStr28 = \frac{Str28}{MaxStr28} \tag{16}$$

At age *X*, *StrX* is the compressive strength for a given SO_3/CL, *MaxStrX* is the maximum strength of the cement type, *RelStrX* is the relative strength for a value of SO_3/CL, and *X* = 7 or 28. Figure 1a,b depict the relative 7- and 28-day strengths as a function of SO_3/CL, proving that a single distribution can describe the results of the four CEM types.
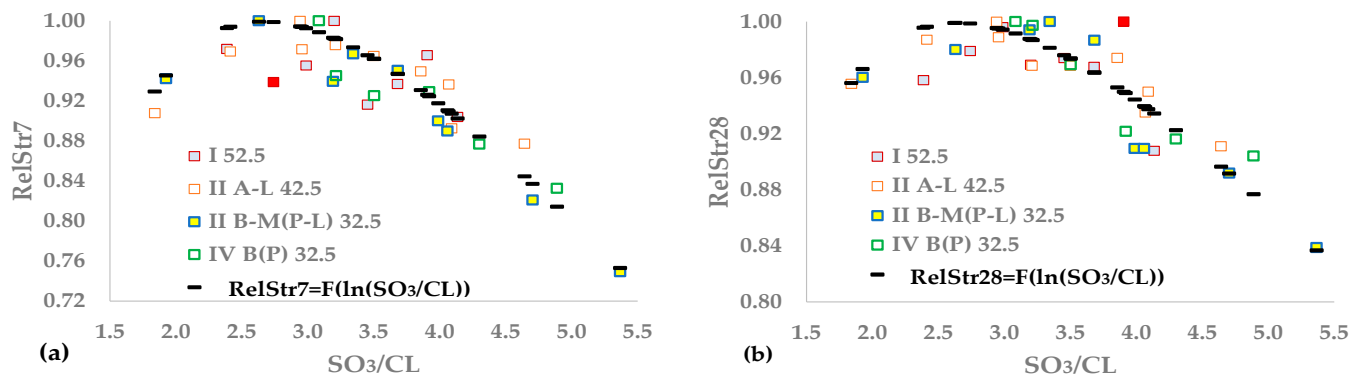

Figure 1. Functions between SO_3/CL and (**a**) *RelStr7* or (**b**) *RelStr28*.

The initial processing stage was applied to the parabolic Equations (17) and (18) to correlate the 7- and 28-day relative strengths with SO_3/CL: SO_3/CL was the independent variable for the first equation, resulting in a symmetric curve around the maximum, and $ln(SO_3/CL)$ was the independent variable for the second equation, taking into account the asymmetry of these experimental data. Equations (19) and (20) calculate the optimum SO_3/CL of (17) and (18). For the optimal value, $RelStrX(SO_3/CL_{opt})$ shall be equal to 1. Constraint (21) guarantees the above values.

$$RelStrX = A_2 \cdot \left(\frac{SO_3}{CL} \right)^2 + A_1 \cdot \left(\frac{SO_3}{CL} \right) + A_0 \tag{17}$$

$$RelStrX = B_2 \cdot \left(\ln\left(\frac{SO_3}{CL} \right) \right)^2 + B_1 \cdot \left(ln\left(\frac{SO_3}{CL} \right) \right) + B_0 \tag{18}$$

$$\frac{SO_3}{CL}_{Opt} = -\frac{A_1}{2 \cdot A_2} \tag{19}$$

$$\frac{SO_3}{CL}_{Opt} = exp\left(-\frac{B_1}{2 \cdot B_2} \right) \tag{20}$$

$$0.999 \leq RelStrX\left(\frac{SO_3}{CL}_{Opt} \right) \leq 1.001 \tag{21}$$

The optimal coefficients of (17) and (18) were estimated through minimizing the residual error, with the Generalized Reduced Gradient algorithm used at this stage. For each model, Equations (22) and (23) provide the residual error, s_{Res}, and coefficient of determination, R^2, respectively. Our algorithm used the error, s_{Opt}, which is given in Equation (24), to assess whether a model satisfactorily approximates the sulfate optimum.

$$s_{Res}^2 = \sum_{I=1}^{M} \left(RelStrX(I) - RelStrX_{Calc}(I) \right) \Big/ (M-k) \; I = 1 \; to \; M \tag{22}$$

$$R^2 = \left(1 - \frac{s_{Res}^2}{s_{Exp}^2} \right) \tag{23}$$

$$s_{Opt}^2 = \sum_{j=1}^{Nopt} \left(RelStrX(J) - RelStrX_{Calc}(J)\right)\Big/ N_{opt} \; J = 1 \; to \; N_{opt} \tag{24}$$

$$where \; RelStrX(J) \geq 0.99$$

M is the number of the experimental points $RelStrX(I)$ for $X = 7$ or 28 and $I = 1$ to M, while $RelStrX_{Calc}(I)$ are the corresponding computed values for each model. s_{Exp} is the standard deviation of the population of $RelStrX$, and k represents the degrees of freedom of the applied equation. The number of variables in (18) and (19) is three; however, $k = 2$ since both models are subject to the constraint (22). N_{opt} is the count of $RelStrX$ that is greater or equal to 0.99. Table 8 demonstrates the optimal coefficients A_i, B_i, with $i = 0$, 1, or 2, as well as the SO_3/CL_{Opt}, s_{Res}, s_{Exp}, s_{Opt}, and R^2 for each model. The algorithm permits up to 1 outlier out of the 33 experimental points when the absolute difference between actual and computed values is higher than $2s_{Res}$.

Table 8. Coefficients and statistics of parabolic model.

	ResStrX = F(SO_3/CL)			ResStrX = F(ln(SO_3/CL))	
	ResStr7	**ResStr28**		**ResStr7**	**ResStr28**
A_0	0.9269	0.9271	B_0	0.5139	0.6918
A_1	0.0754	0.0673	B_1	0.9888	0.6315
A_2	−0.0197	−0.0157	B_2	−0.5039	−0.3246
s_{Res}	0.0252	0.0208	s_{Res}	0.0234	0.0177
s_{Exp}	0.0552	0.0400	s_{Opt}	0.0552	0.0400
s_{Opt}	0.0250	0.0154	s_{Exp}	0.0110	0.0101
R^2	0.792	0.726	R^2	0.821	0.802
SO_3/CL_{Opt}	1.91	2.14	SO_3/CL_{Opt}	2.67	2.65

Table 8 results show that using the logarithm of SO_3/CL as an independent variable covers a part of the data asymmetry. In both the 7- and 28-day strengths, the logarithmic model has a higher R^2 than the symmetric parabolic equation and more effectively approximates the maximum strength values that show smaller s_{Opt} values. In Figure 1a,b, black dashes indicate calculated values using the asymmetric equation, and red points depict outliers. For 7-day strength, optimum $SO_3/CL = 2.67$ seems reasonable, though it is probably found to the left of the closest approximation. In Figure 1b, all points with $RelStr28 \geq 0.99$ are found to the right of the best approximation. Therefore, there is an underestimation of the optimal value, and a better model is necessary. We implemented shallow neural networks (ANN) with one hidden layer to overcome this discrepancy.

The input vector X contains the SO_3/CL values, and the output vectors $RelStrX$ are the 7- and 28-day relative strengths. The dimension of the vectors is M. Equation (25) provides the respecting normalized variable XN, where X_{MIN} and X_{MAX} are the minimum and maximum values of the SO_3/CL. The output vectors are already normalized because their values continuously belong to the interval [0, 1]. The hidden layer has N_N nodes using the sigmoid equation as an activation function, which were provided in Equation (26). Equation (27) gives the input Z_J to each node, where W_{0J} and W_{1J} are the biases and the synaptic weights between the input and the hidden layer, respectively. Finally, Equation (28) calculates the values of $RelStrX_{Calc}$, where V_J are the synaptic weights between the hidden layer and the output.

$$XN = \frac{X - X_{MIN}}{X_{MAX} - X_{MIN}} \tag{25}$$

$$\alpha(Z_J) = \frac{1}{1 + \exp(-Z_J)} \; J = 1 \; to \; N_N \tag{26}$$

$$Z_J = W_{0J} + W_{1J} \cdot XN \; J = 1 \; to \; N_N \tag{27}$$

$$RelStrX_{Calc} = \sum_{J=1}^{N_N} V_j \cdot \alpha(Z_J) \tag{28}$$

Through the Generalized Reduced Gradient algorithm, we estimated the synaptic weights of Equations (27) and (28) by minimizing the residual error of Equation (22), s_{ResJ}, for all experimental data. The minimum s_{Res} occurs when the number of nodes in the hidden layer $N_N = 2$. Therefore, the continuous ANN function results in the Formulae (29), where Xn is a continuous variable belonging to the interval $[X_{MIN}, X_{MAX}]$. The numerical optimization problem contains two constraints for the optimal Xn: the value of the ANN function for this point should be close to 1, and the derivative should be close to 0. Equation (30) expresses these two constraints. The freedom degrees in Equation (22) are k = 6 − 2 = 4 due to these constraints.

$$F_{ANN}(XN) = \sum_{j=1}^{2} \frac{V_J}{1 + exp\left(-\left(W_{0J} + W_{1J} \cdot XN\right)\right)} \; ; \; XN = \frac{Xn - X_{MIN}}{X_{MAX} - X_{MIN}} \tag{29}$$

$$-0.01 \le F'_{ANN}(Xn_{Opt}) \le 0.01; \; 0.999 \le F_{ANN}(Xn_{Opt}) \le 1.001 \tag{30}$$

Table 9 demonstrates the synaptic weights and statistics of the two ANNs, while Figure 2a,b illustrates the fitting of the ANNs results to the experimental data. Applying neural networks with one hidden layer and two nodes improves all statistics compared to logarithmic equations. For the 28-day relative strength, the improvements are 5.5% for s_{Res}, 2.6% for R^2, and 91.2% for s_{Opt}, i.e., the ANNs more effectively approximate both the shape of the experimental curve and the optimum SO_3. The same conclusion emerges from Figure 2a,b. The optimal SO_3/CL increases with the age of the mortar ($SO_3/CL_{28\text{-}day} > SO_3/CL_{7\text{-}day}$), which confirms the previous studies' findings [15,35,40,41].

Table 9. Synaptic weights and statistics of ANNs.

	$ResStr7 = F_{ANN}(Xn)$	$ResStr28 = F_{ANN}(Xn)$
V_1	0.1572	0.1685
W_{01}	−2.724	−2.986
W_{11}	17.33	14.82
V_2	1.016	4242
W_{02}	2.211	−8.399
W_{12}	−1.834	−0.3446
s_{Res}	0.0227	0.0167
s_{Exp}	0.0552	0.0400
s_{Opt}	0.0095	0.0053
R^2	0.831	0.823
SO_3/CL_{Opt}	2.85	3.00

The residual errors shown in Table 9, which were computed using all experimental data, are training errors, s_{train}. To estimate the test error (s_{Test}), as well as due to the limited number of data ($M = 33$), we applied the following procedure for the 28-day ANN: (a) the training set contains M-1 datasets, and the remaining set is used for testing; (b) the non-linear regression technique calculates the optimal parameters of the training set and its s_{Res}; (c) we compute the value of the test set using these synaptic weights, the input value, and Equation (29); (d) the difference between the experimental and the calculated test value is the error, s_T, of the test; (e) the algorithm considers all possible combinations of training and test sets, resulting in M datasets of both types; and (f) Equation (31) provides the training and test errors, taking into account the error of each dataset.
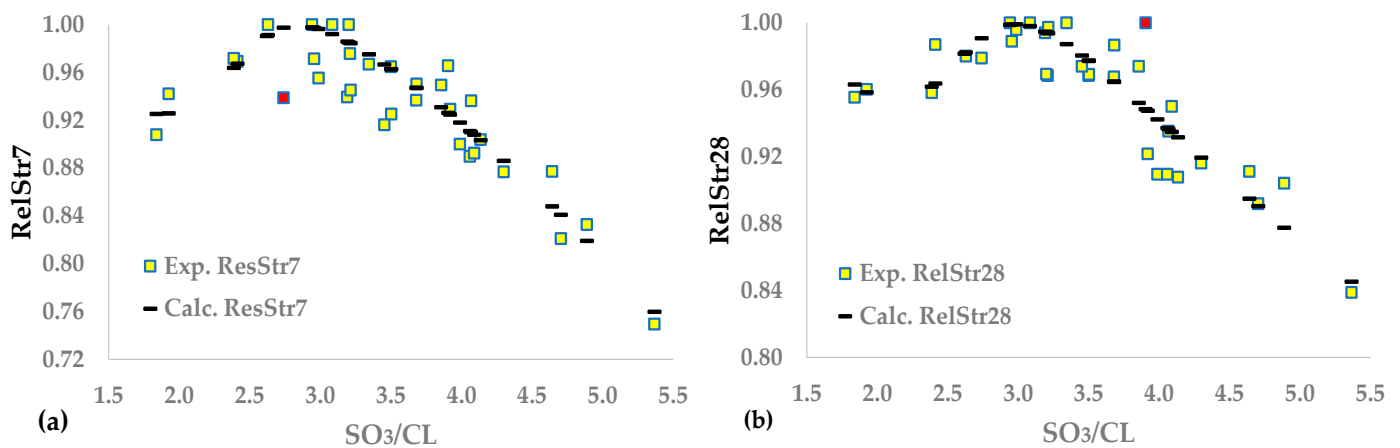
Figure 2. Neural network functions between SO_3/CL and (**a**) *RelStr7* or (**b**) *RelStr28*.

$$s^2_{Train} = \sum_{I=1}^{M} s^2_{Res}(I) \Big/ M \; ; \; s^2_{Test} = \sum_{I=1}^{M} s^2_T(I) \Big/ M \tag{31}$$

The algorithm for the 28-day relative strength gives the following results: s_{Train} = 0.0167, and s_{Test} = 0.0172. The coefficient of determination, R^2, of the test set is 0.813. By applying the same procedure to the logarithmic model, the R^2 of the test set is 0.793, proving that the implementation of ANNs causes a significant improvement in all investigated statistics.

3.2. Correlation of Strength with Sulfates and Clinker Mineral Phases

According to the literature, a function exists between the SO_3 optimum and the C_3S and C_3A of clinker [14–16,22,24,25,33,40]. Figure 3a,b shows the relationship between the 28-day relative strength and the ratio of either (a) moles SO_3/moles C_3A (MSO_3/C_3A) or (b) moles SO_3/moles C_3S (MSO_3/C_3S), in a similar way to the method shown in Figure 1a,b. The correlation includes the mineral phases of the clinker contained in the cement, which is initially computed via the Bogue formula and shown in Table 2. Equations (32) calculate the two mentioned molecular ratios, where MW_{SO3} = 80, MW_{C3A} = 270, and MW_{C3S} = 228 are the molecular weights of SO_3, C_3A, and C_3S, respectively.

$$\frac{MSO_3}{C_3A} = \frac{\frac{SO_3}{CL}}{MW_{SO3}} \Big/ \frac{C_3A}{MW_{C3A}}; \; \frac{MSO_3}{C_3S} = \frac{\frac{SO_3}{CL}}{MW_{SO3}} \Big/ \frac{C_3S}{MW_{C3S}} \tag{32}$$
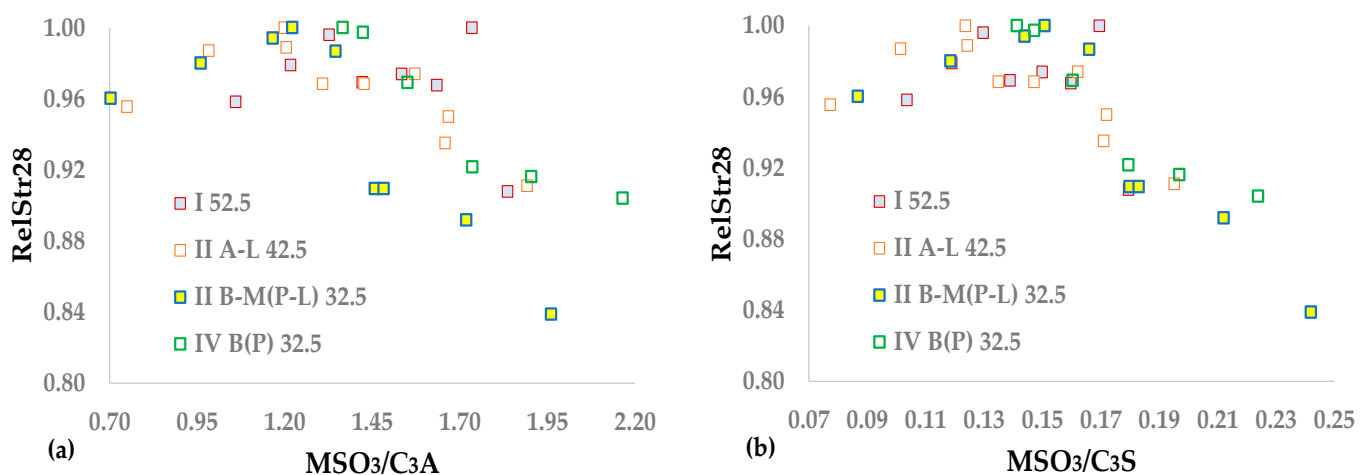

Figure 3. Functions between (**a**) MSO_3/C_3A and (**b**) MSO_3/C_3S and *RelStr28*.

Figure 3a,b show that a single distribution can describe the results of the four CEM types. However, the scattering of the points is higher than that observed in Figure 1b because the two independent inputs combine three measured or calculated variables, resulting in a higher level of uncertainty. The two plots are not symmetrical around their maximum values. Thus, the ANN model, which was successfully applied in Section 3.1, is appropriate. The algorithm implements the set of Equations (25)–(30) where the vector X is either the vector of MSO_3/C_3A or MSO_3/C_3S, while Xn_{opt} corresponds to the optimal position of each variable. Table 10 shows the synaptic weights and statistics of the two ANNs correlating *RelStr28*, with the mineral phases of the clinker calculated using XRF analysis and the Bogue formulae.

Table 10. Synaptic weights and statistics of ANNs using C_3A and C_3S as inputs (Bogue formulae).

	ResStr28 = $F_{ANN}(MSO_3/C_3A)$	*ResStr28 = $F_{ANN}(MSO_3/C_3S)$*
V_1	0.1889	0.1916
W_{01}	−2.960	−2.762
W_{11}	12.72	13.62
V_2	4230	4248
W_{02}	−8.393	−8.400
W_{12}	−0.3604	−0.4023
s_{Res}	0.0241	0.0161
s_{Exp}	0.0400	0.0400
s_{Opt}	0.0065	0.0087
R^2	0.633	0.835
Xn_{Opt} (MSO_3/C_3A_{Opt} or MSO_3/C_3S_{Opt})	1.25	0.132

The algorithm permits up to 2 outliers out of the 33 experimental points because of the higher uncertainty of the input variables, compared to the ANN correlating *RelStr28* and SO_3/CL. Figure 4a,b depicts the fitting of the ANNs results to the experimental data. $F_{ANN}(MSO_3/C_3A)$ presents a low R^2, and the model is unreliable. In contrast, $F_{ANN}(MSO_3/C_3S)$ has satisfactory statistics close to those of $F_{ANN}(SO_3/CL)$. Furthermore, the two outliers (red points) of Figure 4b are at a distance of ~$3s_{Res}$ from the calculated points.
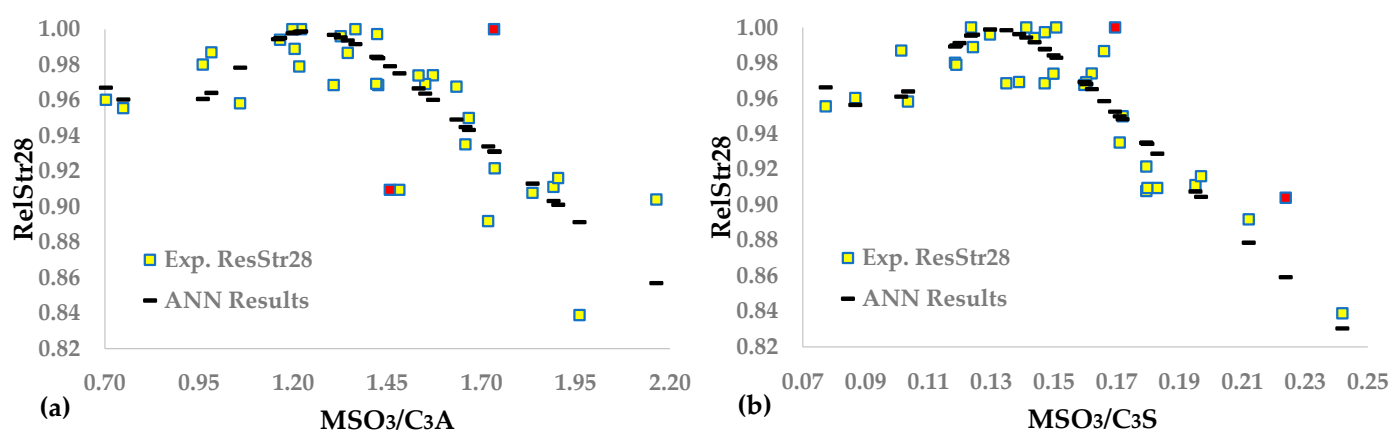

Figure 4. Neural network functions between (**a**) MSO_3/C_3S and (**b**) MSO_3/C_3S and *RelStr28*.

We repeated the procedure that uses the mineral constituents directly determined via XRD to investigate the accuracy of data fitting and the position of the optimum sulfates. We implemented all ANNs, except for total C_3A_{XRD} and C_3S_{XRD}, as well as M_1 C_3S_{XRD}, which

is more reactive, according to the literature [40,52]. Table 2 shows the values of these phases measured via XRD, and Equation (33) calculates the corresponding three molecular ratios.

$$\frac{MSO_3}{C_3A_{XRD}} = \frac{\frac{SO_3}{CL}}{MW_{SO3}} \Big/ \frac{C_3A_{XRD}}{MW_{C3A}}; \quad \frac{MSO_3}{C_3S_{XRD}} = \frac{\frac{SO_3}{CL}}{MW_{SO3}} \Big/ \frac{C_3S_{XRD}}{MW_{C3S}};$$
$$\frac{MSO_3}{M_1C_3S_{XRD}} = \frac{\frac{SO_3}{CL}}{MW_{SO3}} \Big/ \frac{M_1C_3S_{XRD}}{MW_{C3S}} \tag{33}$$

Table 11 demonstrates the synaptic weights and the statistics of the three ANNs correlating *RelStr28*, with the mineral phases of the clinker determined via XRD analyses.

Table 11. Synaptic weights and statistics of ANNs using C_3A_{XRD}, $C3S_{XRD}$, and $M_1C_3S_{XRD}$.

	RelStr28 = $F_{ANN}(X)$		
	$F_{ANN}(MSO_3/C_3A_{XRD})$	$F_{ANN}(MSO_3/C_3S_{XRD})$	$F_{ANN}(MSO_3/M_1C_3S_{XRD})$
V_1	0.1785	0.2260	0.2174
W_{01}	−2.721	−2.537	−2.574
W_{11}	13.44	11.59	11.67
V_2	4241	4241	4147
W_{02}	−8.404	−8.405	−8.384
W_{12}	−0.3444	−0.4396	−0.4111
s_{Res}	0.0162	0.0164	0.0203
s_{Exp}	0.0400	0.0400	0.0400
s_{Opt}	0.004	0.0064	0.0056
R^2	0.833	0.830	0.738
Xn_{Opt} (MSO_3/C_3A_{XRDOpt} or MSO_3/C_3S_{XRDOpt} or $MSO_3/M_1C_3S_{XRDOpt}$	1.55	0.135	0.230

Figure 5a–c depicts the experimental and calculated data using the three ANNs. Comparing the coefficients of determination of $F_{ANN}(MSO_3/C_3A_{XRD})$ and $F_{ANN}(MSO_3/C_3A)$, we observed that the R^2 of the former model is much higher than that of the latter model, before concluding that determining C_3A via XRD results in adequate data fitting and reliable approximation of the optimal sulfates. $F_{AA}(MSO_3/C_3S_{XRD})$ and $F_{AA}(MSO_3/C_3S)$ fit both similarly and satisfactorily to experimental data, and their optimal molecular ratio of SO_3 to mineral phase is roughly the same. The R^2 of $F_{ANN}(MSO_3/M_1C_3S_{XRD})$ is relatively low, though the s_{Opt} is sufficiently reasonable. Therefore, the corresponding optimal molecular ratio could be an initial approximation of the optimum SO_3.
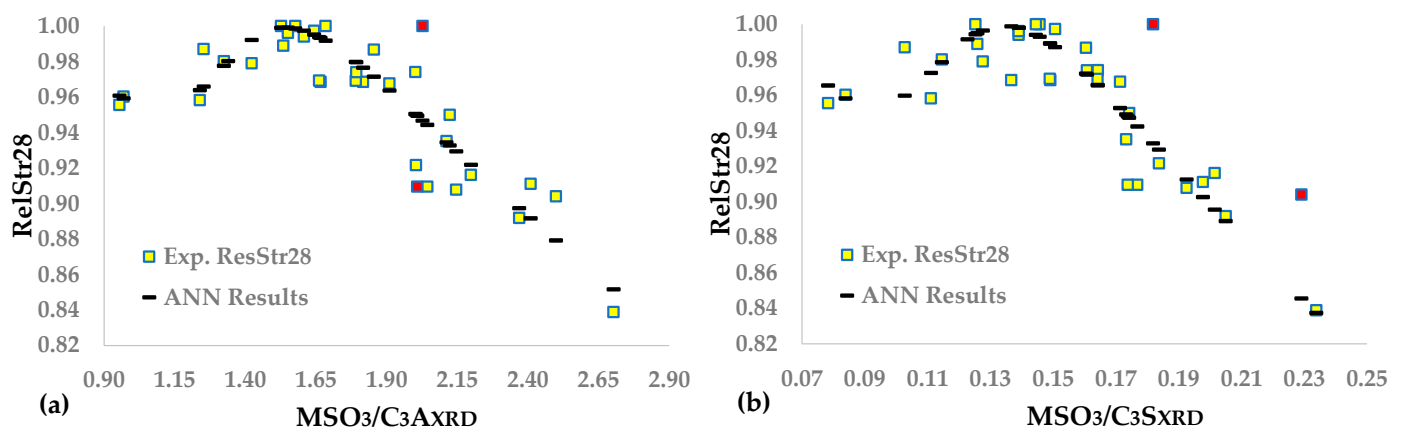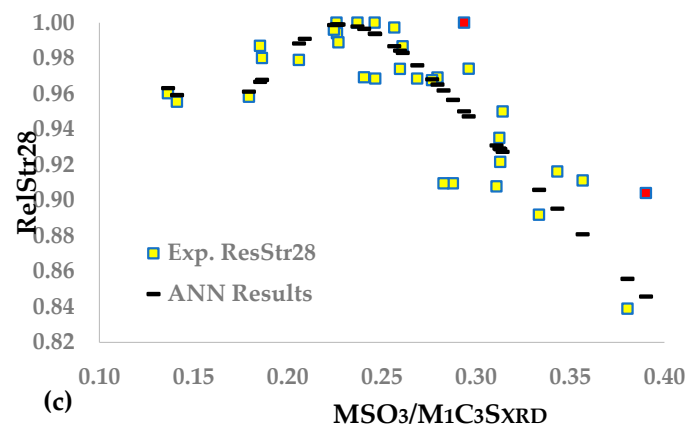

(a)

(b)

Figure 5. *Cont.*

Figure 5. Neural network functions between following models: (**a**) MSO_3/C_3A_{XRD}; (**b**) MSO_3/C_3S_{XRD}; (**c**) $MSO_3/M_1C_3S_{XRD}$ and *RelStr28*.

3.3. Correlation of Strengh with Sulfates and Clinker Content under Selected Size

In Section 3.1, we investigated the function between compressive strength and the factor $\%SO_3/CL$, considering the total clinker content of each cement sample. We tried to evaluate whether some finer part of the clinker improved the relationship between the *RelStr28* and the variable SO_3/CL because it contributed substantially to the 28-day strength, thus applying the subsequent procedure.

(a) We considered the %clinker content to be passing a size (40 μ, 32 μ), $CLPass_j$, as given in Equation (34). The symbols j, $CompPass_{1,j}$, and R_j are the same in Formulas (13) and (34). The upper part of Table 5 shows the values of $CompPass_{1,j}$ for the samples of low and high gypsum and the four CEM types.

$$CLPass_j = CompPass_{1,j} \cdot \left(1 - \frac{R_j}{100}\right) j = 1, 2 \tag{34}$$

(b) CLL_j and CLH_j denote the %clinker passing the sieve j for the low and high gypsum samples. We used the linear combination (35) to calculate the %clinker passing, CLP_j, for each mix of percentages P and 100-P of low and high gypsum samples. Table 7 provides these proportions for all CEM types.

$$CLP_j = \left(P \cdot CLL_j + (100 - P) \cdot CLH_j\right) / 100 \; j = 1, 2 \tag{35}$$

(c) We attempted two correlations using CLP_1 and CLP_2 at 40 μ and 32 μ. Equation (36) provides the two independent variables of the two ANN functions.

$$\frac{SO_3}{CLP}_{Sj} = 100 \cdot {SO_3}\big/{CLP_j} \; j = 1, 2; \; S_1 = 40; \; S_2 = 32 \tag{36}$$

Table 12 provides the synaptic weights and statistics of the two functions between *RelStr28* and clinker content under 40 μ and 32 μ, while Figure 6a,b depicts the fitting of the ANNs results to the experimental data. The calculation permits up to two outliers because the independent variables arise from more chemical analyses and physical measurements (sieving) than SO_3/CL, resulting in higher uncertainty.

Table 12. Synaptic weights and statistics of ANNs.

	$ResStr28 = F_{ANN}(SO_3/CLP_{40})$	$ResStr28 = F_{ANN}(SO_3/CLP_{32})$
V_1	0.1832	0.1853
W_{01}	−2.844	−2.679

Table 12. *Cont.*

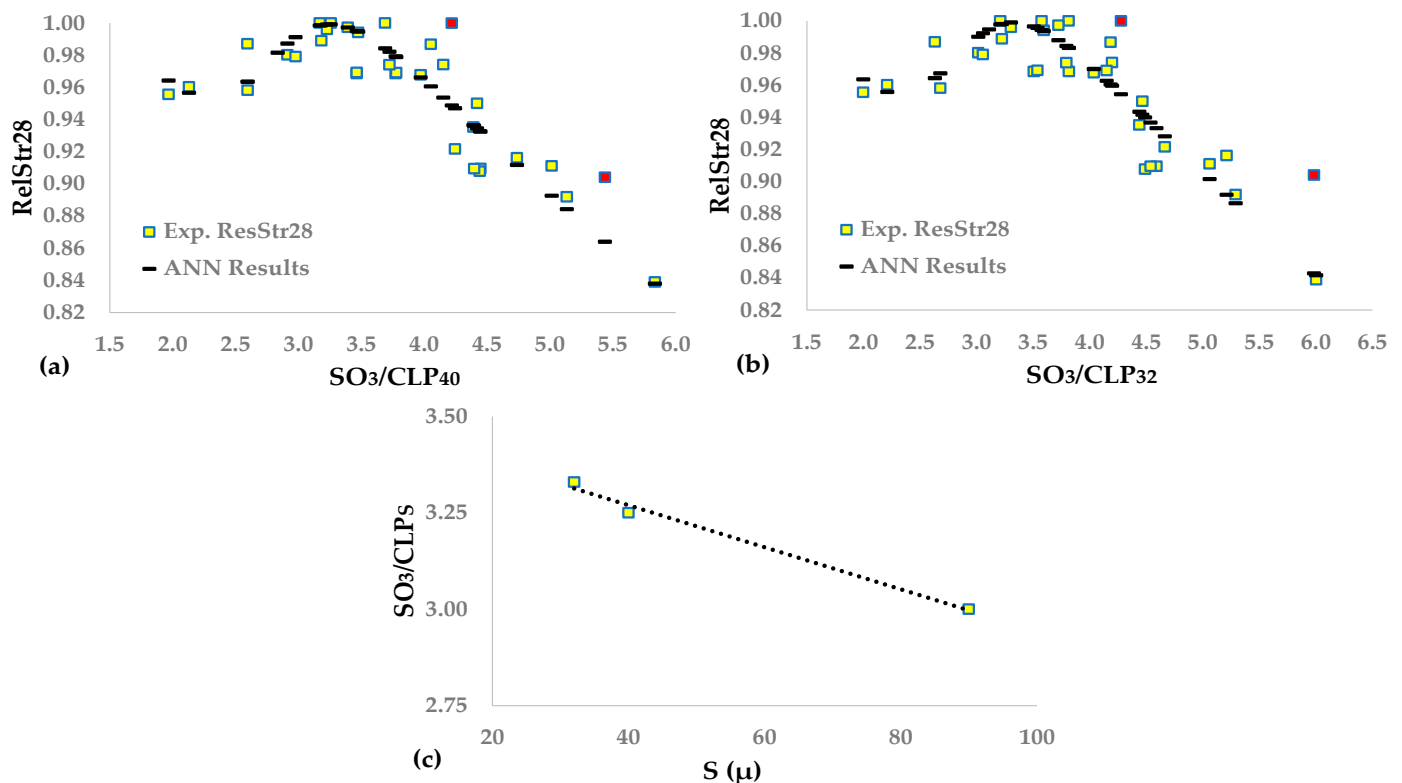|	*ResStr28 = $F_{ANN}(SO_3/CLP_{40})$*	*ResStr28 = $F_{ANN}(SO_3/CLP_{32})$*
W_{11}	13.94	13.32
V_2	43.87	83.92
W_{02}	−3.806	−4.468
W_{12}	−0.3836	−0.3751
s_{Res}	0.0162	0.0166
s_{Exp}	0.0400	0.0400
s_{Opt}	0.0067	0.0083
R^2	0.835	0.826
SO_3/CLP_{Opt}	3.25	3.33

Figure 6. Neural network functions between (**a**) SO_3/CLP_{40}, (**b**) SO_3/CLP_{32}, and *RelStr28*. (**c**) Function between SO_3/PCL_S and sieve opening size S.

We derived the following conclusions by comparing Tables 11 and 12 and Figures 2b and 6a,b.

(a) The total clinker content of the cement is the %clinker in a sieve where the passing is 100%, e.g., 90 microns, as well as $SO_3/CL = SO_3/CLP_{90}$. Thus, the three ratios, i.e., SO_3/CL_{90}, SO_3/CLP_{40}, and SO_3/CLP_{32}, express the clinker content of cement under some sieve.

(b) There is an approximate linear increase in the optimal ratio SO_3/CLP_S when the sieve size, S, decreases from 90 μ to 32 μ, as shown in Figure 6c.

(c) $F_{AA}(SO_3/CL)$ and $F_{AA}(SO_3/CLP_{40})$ have a similarly good fit to the experimental data, though the second ANN has a higher R^2, making it probably preferable.

(d) $F_{AA}(SO_3/CLP_{32})$ seems to be the worst model. Its s_{Opt} is higher than those the other two models, and despite accepting two outliers, the R^2 is the same as that of $F_{AA}(SO_3/CL)$.

(e) Based on this model, one could conclude that cement hydration in 28 days proceeds to create clinker grains coarser that are than 32 microns, meaning that $F_{AA}(SO_3/CL)$

and $F_{AA}(SO_3/CLP_{40})$ provide a more accurate fitting to the data and a closer approximation to the optimal SO_3.

(f) The fraction between 3 and 32 microns is critical in achieving maximum 28-day strength, according to Celic [53]. Table 5 results show that P32-R3 ranges between 59.4 and 66.9%. The literature [54] states that the optimum fraction is 70%. If the CEM types studied had such P32–R3, the relationship between *RelStr28* and CLP_{32} might improve.

3.4. Summary of Results

Table 13 summarizes the optimal sulfate ratios for ANNs with $R^2 \geq 0.82$. As s_{Res} is around 0.016 for all ANNs, as well as to achieve an estimation of the confidence interval of each optimum, we considered the ratios to the left and right of the optimal value, where *ResStr28* = 0.98. A second check concerned the compatibility of the optimal sulfates calculated from the six ANNs for each CEM type. The algorithm used Tables 2, 6 and 7 and Equation (35) to determine the average C_3S, C_3S_{XRD}, and C_3A_{XRD} and the average percentages of Clinker, CLP_1, and CLP_2 for each CEM type. Next, it calculated the optimal SO_3 content per model and CEM type. Table 13 shows these results.

Table 13. Summary of results and optimal SO_3 (%) of ANNs.

	ANN Model Using					
	SO_3/CL	SO_3/CL_{40}	SO_3/CL_{32}	MSO_3/C_3S	MSO_3/C_3S_{XRD}	MSO_3/C_3A_{XRD}
Optimal SO_3 ratio	3.00	3.25	3.33	0.132	0.135	1.55
Low ratio for *ResStr28* = 0.98	2.60	2.82	2.86	0.113	0.115	1.34
High ratio for *ResStr28* = 0.98	3.46	3.76	3.89	0.153	0.156	1.79
Optimal SO_3 (%) for						
I 52.5 N	2.7	2.7	2.8	2.7	2.7	2.7
II A-L 42.5 N	2.3	2.3	2.4	2.3	2.3	2.3
II B-M (P-L) 32.5 N	2.0	2.0	2.0	2.0	2.0	2.0
IV B (P) 32.5 N	1.7	1.7	1.8	1.7	1.8	1.8

Table 13 shows that the low and high ratios for *RelStr28* = 0.98 are not symmetrical around the optimum because the distributions are asymmetrical. The six models closely approximated the SO_3 optimum, providing roughly the same value per CEM type. Therefore, the ANNs are reliable for the studied clinker mineralogy and cement fineness.

3.5. Uncertainty Analysis

All developed models indicate that SO_3 content affects compressive strength. Approximating the optimal location is critical to cement plant quality control. In this context, the SO_3 variance can impact the strength variance. An analytical error propagation model can facilitate a quantitative correlation between these variances. The variance of y, σ_y^2, of an analytical function $y = f(x_1, x_2, \ldots, x_n)$ can be determined using those of independent variables x_i, σ_i^2 when applying Equation (37).

$$\sigma_y^2 = \sum_{i=1}^{n} \left(\frac{\partial y}{\partial x_i}\right)^2 \cdot \sigma_{xi}^2 \tag{37}$$

We implemented the error propagation equation for the models $RelStr28 = F_{ANN}(SO_3/CL)$ and $RelStr28 = F_{ANN}(MSO_3/C_3S)$. The independent variables of the first model were the SO_3 content, the clinker fraction CL = %Clinker/100, and laboratory reproducibility in 28-day strength measurement, σ_R. The second model used the C_3S content as an additional input. Equation (38) gives the derivatives of (29).

$$\frac{\partial F_{ANN}}{\partial XN} = \sum_{j=1}^{2} \frac{V_J \cdot W_{1J} \cdot exp\left(-(W_{0J} + W_{1J} \cdot XN)\right)}{\left(1 + exp\left(-(W_{0J} + W_{1J} \cdot XN)\right)\right)^2} \; ; \; \frac{\partial XN}{\partial Xn} = \frac{1}{X_{MAX} - X_{MIN}} \tag{38}$$

If $Xn = SO_3/CL$, the partial derivatives of SO_3 and CL are:

$$\frac{\partial Xn}{\partial SO_3} = \frac{1}{CL}; \frac{\partial Xn}{\partial CL} = \frac{-SO_3}{CL^2} \qquad (39)$$

Otherwise, if $Xn = MSO_3/C_3S$, the derivatives of the three variables are:

$$\frac{\partial Xn}{\partial SO_3} = \frac{MW_{C3S}}{MW_{SO3}\cdot CL\cdot C_3S}; \frac{\partial Xn}{\partial CL} = \frac{-SO_3\cdot MW_{C3S}}{MW_{SO3}\cdot CL^2\cdot C_3S}; \frac{\partial Xn}{\partial C_3S} = \frac{-SO_3\cdot MW_{C3S}}{MW_{SO3}\cdot CL\cdot C_3S^{\,2}} \qquad (40)$$

Equations (41) and (42) give the 28-day strength variances, $\sigma^2{}_{Str28}$, of the two models.

$$\sigma_{Str28}^2 = \left(\left(\frac{\partial F_{ANN}}{\partial XN}\cdot\frac{\partial XN}{\partial Xn}\right)^2\cdot\left(\left(\frac{\partial Xn}{\partial SO_3}\cdot\sigma_{SO3}\right)^2 + \left(\frac{\partial Xn}{\partial CL}\cdot\sigma_{CL}\right)^2\right) + \sigma_R^2\right)\cdot MaxStr28 \quad (41)$$

$$\sigma_{Str28}^2 = \left(\left(\frac{\partial F_{ANN}}{\partial XN}\cdot\frac{\partial XN}{\partial Xn}\right)^2\cdot\left(\left(\frac{\partial Xn}{\partial SO_3}\cdot\sigma_{SO3}\right)^2 + \left(\frac{\partial Xn}{\partial CL}\cdot\sigma_{CL}\right)^2 + \left(\frac{\partial Xn}{\partial C_3S}\cdot\sigma_{C3S}\right)^2\right) + \sigma_R^2\right)\cdot MaxStr28 \quad (42)$$

We applied the error propagation equations for CEM II A-L 42.5 N, with $MaxStr28 = 54$ MPa, $CL = 0.775$, and $C_3S = 64.7\%$, while also assuming the following values for the input standard deviations: $\sigma_{CL} = 0.02$, $\sigma_{C3S} = 2$, $\sigma_R = 0.02$, SO_3 of cement from 2% to 3% with a step of 0.1%, and σ_{SO3} from 0.05% to 0.3%, increasing in steps of 0.05%. Figure 7a,b show the standard deviation σ_{Str28} as a function of SO_3 and σ_{SO3} for the two models investigated.
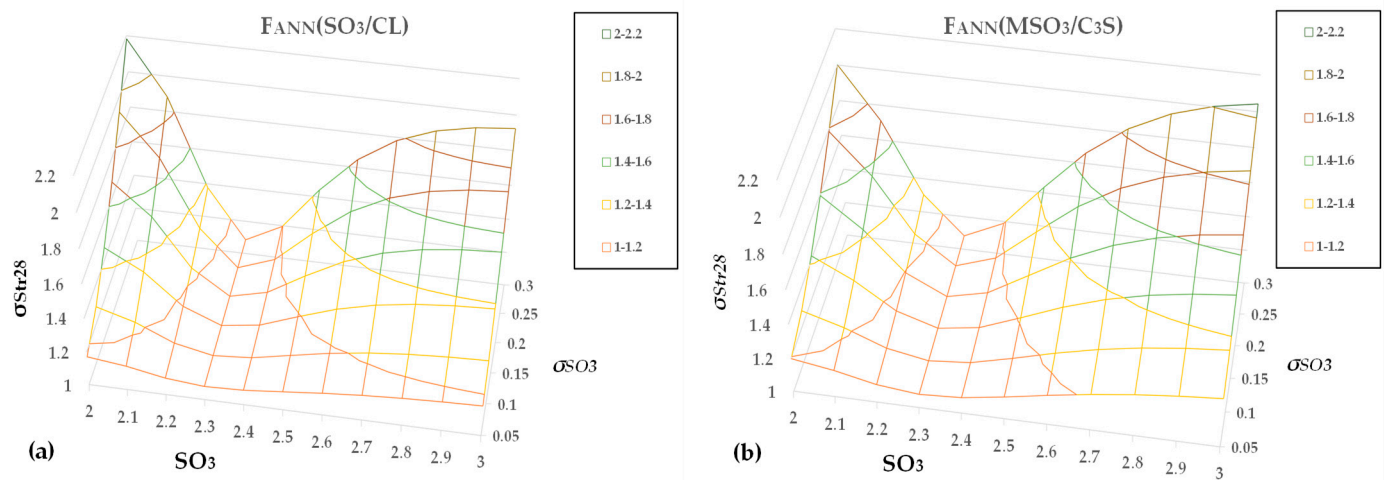

Figure 7. σ_{Str28} as a function of SO_3 and σSO_3 for models (**a**) $F_{ANN}(SO_3/CL)$ and (**b**) $F_{ANN}(MSO_3/C_3S)$.

The two figures lead to the following remarks.

(a)   The shape of the functions is similar for both models, making the joint conclusions more reliable.

(b)   If the location of the SO_3 target is near the optimum value and realized independently of the SO_3 standard deviation, the 28-day strength variance remains low. Therefore, an adequate approximation of the optimal sulfate achieves two goals: maximum strength and reduced strength variance, regardless of SO_3 variation.

(c)   As the SO_3 value differs from the optimum value, an increase in SO_3 variance leads to a deterioration of strength variability. For $SO_3 = 2.9\%$, an increase in σ_{SO3} from 0.05 to 0.2 causes an increase in σ_{Str28} from 1.2 to 1.5 for the first model and from 1.3 to 1.6 for the second model.

(d)   The above remarks necessitate an automatic controller that regulates SO_3 using gypsum dosing to achieve the SO_3 target with minimum variance, like the model presented in the literature [46].

(e)   In Figure 7a,b, the surfaces are not symmetrical around the optimal line $\sigma_{SO3} = f(SO_{3opt})$, where SO_{3opt} denotes the optimal sulfate. The left side slope is steeper than the right, meaning that if $SO_3 < SO_{3opt}$, the deterioration in σ_{Str28} variance is more substantial than in $SO_3 > SO_{3opt}$.

4. Conclusions

This study attempts to approximate the optimal sulfate content of cement exclusively using cement manufactured in closed-circuit industrial mills. The advantage of this technique is that the obtained samples have the same properties (fineness, composition, forms of the sulfate carriers, and interaction of the grinding aid with the solids) as those of the cement produced. Additionally, the particle distribution of each component within each sample results from the actual production process, which is almost impossible to accomplish via grinding in a laboratory mill. The experimental design includes physical, chemical, and mechanical tests on four CEM types containing up to three main components, except gypsum, and the raw materials. The sampling was realized within two months to allow the clinker mineral composition to incorporate actual production variations. The plant laboratory took two samples of low and high gypsum for each CEM type by keeping constant the clinker content, before mixing the samples in conventional proportions to obtain new samples with a gradual increase in SO_3. After air jet sieving, XRF analysis provided the chemical composition of the specimens and their residues at each sieve size. The solution of a system of equations provides the %components of the above. The main conclusions of this study are as follows.

(1)   A unique curve can express the function between relative compressive strength and the ratio between sulfate and clinker content—SO_3/CL—for all CEM types. This conclusion holds for both the total clinker and the clinker passing the 40 μ and 32 μ sieves of cement. A parabolic equation between relative compressive strength and SO_3/CL can fit the experimental data. Using the logarithm of SO_3/CL as an independent variable, the equation provides a better R^2 than the simple parabola because it covers a part of the data asymmetry. However, the logarithmic model underestimates the optimal SO_3/CL position for both 7- and 28-day strength.

(2)   A shallow ANN with one hidden layer and two nodes provides a better R^2 in training and test sets, as well as a closer approximation of the optimal SO_3/CL than the simple second-order models. The numerical algorithm for determining the synaptic weights comprises two constraints for the maximum value and its derivative. The optimal SO_3/CL is 2.85 for the 7-day strength and 3.0 for the 28-day strength.

(3)   The ANN using the clinker passing at 40 μ in the sulfate to clinker ratio, SO_3/CLP_{40}, gives equivalently reliable results to the first fundamental ANN with SO_3/CLP_{40Opt} = 3.25. The corresponding ANN using the clinker passing through a 32 μ sieve seems to be the worst among the three ANNs for the particle distributions of cement samples investigated with SO_3/CLP_{32Opt} = 3.33. $SO_3/CL = SO_3/CLP_{90}$ because all cement specimens were finer than 90 μ. The three optimal sulfate-to-clinker ratios are in good linear agreement with the sieves' grid size.

(4)   The clinker content of the four CEM types varies from 58 to 90%, covering most of modern cement production. The above result means that the implemented ANNs and their approximation to optimal SO_3 can have a relatively broad application, at least as a guide for an experimental design.

(5)   Our research investigated the well-known functions between SO_3, C_3S, and C_3A computed with Bogue formulae and direct measurement via XRD. We expressed the ratio of SO_3 using each mineral phase as a molecular ratio, and we developed the corresponding ANN models between 28-day compressive strength and these variables.

(6)   Determination of C_3A via XRD results in adequate data fitting and reliable approximation of the optimal sulfates. The optimal MSO_3/C_3A_{XRD} is 1.55, though the C_3A range is short for the series of clinkers examined.

(7)   The ANNs using MSO_3/C_3S_{XRD} and MSO_3/C_3S fit both similarly and satisfactorily to experimental data, and their optimal molecular ratio of SO_3 to mineral phase is roughly the same, being 0.135 and 0.132, respectively. The clinkers' C_3S ranged from 61 to 68, covering the majority of good reactivity clinkers manufactured nowadays. The above result means that the developed ANNs and the corresponding approximation of optimum sulfate could have a relatively general implementation. The attempt to correlate 28-day strength with M_1 C_3S, which is measured via XRD, did not perform as well as previous models.

(8)   Particular focus was also given to the impact of SO_3 uncertainty on the 28-day strength variance using the error propagation method. One of the main conclusions is that an adequate approximation to the optimal sulfate achieves two goals: maximum strength and reduced strength variance. An automatic controller regulating SO_3 using gypsum dosing to achieve the SO_3 target with minimum variance is also necessary. Therefore, if a cement plant operates the cement mills, with the SO_3 target being close to optimum, and regulates sulfates with an automatic controller, it can gain significant improvement in the products' quality.

This research proposes some technical novelties concerning a procedure used to approximate the SO_3 optimum on an industrial scale, the tools to obtain it, and optimal ratios of sulfate to several characteristics of cement and clinker. We suggest the exclusive use of industrial cement samples of several CEM types with low and high gypsum and their convenient mixing. Using relative strength and the ratio of SO_3 to a quality parameter, e.g., %clinker, C_3S, etc., normalizes the results, allowing them to appear in a single curve. The developed algorithm successfully used neural networks to fit and reliably predict the results. According to the authors' knowledge, it is hard to find application of ANNs for SO_3 optimization in the literature. We provide approximations of optimum SO_3 as a function of clinker content, %clinker passing through some sieves, C_3S, and C_3A. We calculated some of these functions for a wide interval of input variables' values. Thus, these approximations could have a relatively broad application in daily plant quality control, at least as a guide for experimental design.

The research into the correlation between optimum SO_3 and some main cement characteristics could continue for the relationship between optimal sulfate and cement fineness, using samples of products manufactured in industrial closed-circuit mills.

Appendix A

List of the companies supplying raw materials and main measuring devices

Materials
Clinker and cement: Halyps Building Materials, S. A., Aspropyrgos, Greece.
Raw materials suppliers
Pozzolan: Aegean Perlites S. A., Nissiros, Greece.
Gypsum: George Zervakis S.A.—Gypsum Mines of Eastern Crete, Sitia, Greece.
Limestone: Aragonitis Quarry, Aspropyrgos, Greece.
Grinding Aid: GCP Applied Technologies, Milan, Italy.

Measuring instruments
XRF analyzer: Malvern-Panalytical, Almelo, the Netherlands.
XRD analyzer: Malvern-Panalytical, Almelo, the Netherlands.
Press, mixer, jolting apparatus, molds: Toni Technik, Berlin, Germany.
Air jet sieving apparatus and sieves: Hosokawa Alpine, Augsburg, Germany.
Laser particle size analyzer: Cilas, Orléans, France.

Labs performing the tests
The laboratory of Devnya Cement AD (Devnya, Bulgaria) performed the XRD analyses.
The laboratory of Halyps Building Materials S.A. (Aspropyrgos, Greece) performed the sampling and all remaining physical, chemical, and mechanical tests.

References

1. Lee, F.M. *The Chemistry of Cement and Concrete*, 3rd ed.; Chemical Publishing Company Inc.: New York, NY, USA, 1971; pp. 180–181, 297–298, 303, 308–310.
2. Knappert, J.; Treiber, K.; Seemann, S. Gypsum dehydration potential and mean residence time of a stirred media mill during ultra-fine grinding of cement clinker and gypsum. *ZKG Cem. Lime Gypsum* **2022**, *2*. Available online: https://www.zkg.de/en/artikel/zkg_Gypsum_dehydration_potential_and_mean_residence_time_of_a_stirred_media-3749114.html (accessed on 7 April 2023).
3. Copeland, L.E.; Kantro, D.L. Chemistry of Hydration of Portland Cement at Ordinary Temperature. In *The Chemistry of Cements*, 2nd ed.; Taylor, H.F.W., Ed.; Academic Press Inc.: London, UK, 1972; Volume 1, pp. 313–370.
4. Taherdangkoo, R.; Tian, M.; Sadighi, A.; Meng, T.; Yang, H.; Butscher, C. Experimental Data on Solubility of the Two Calcium Sulfates Gypsum and Anhydrite in Aqueous Solutions. *Data* **2022**, *7*, 140. [CrossRef]
5. Bogue, R.H. *The Chemistry of the Portland Cement*, 2nd ed.; Reinhold Publishing Corporation: London, UK, 1955; pp. 245–250.
6. Mindess, S.; Young, J.F.; Darwin, D. *Concrete*, 2nd ed.; Prentice Hall: Upper Saddle River, NJ, USA, 2003.
7. Niemuth, M. Effect of Fly Ash on the Optimum Sulfate of Portland Cement. Ph.D. Thesis, Purdue University, West Lafayette, IA, USA, December 2012; p. 68. Available online: https://www.researchgate.net/publication/266077758_Effect_of_Fly_Ash_on_Optimum_Sulfate_of_Portland_Cement (accessed on 7 April 2023).
8. Evans, K.A. The Optimum Sulphate Content in Portland Cement. p. 3. Available online: https://tspace.library.utoronto.ca/bitstream/1807/11621/1/MQ29389.pdf (accessed on 7 April 2023).
9. *CEN/TC 51, EN 197-1:2011*; Cement. Part 1: Composition, Specifications and Conformity Criteria for Common Cements. CEN: Brussels, Belgium, 2011; pp. 10–15.
10. *ASTM C150/C150M-22*; Standard Specification for Portland Cement. ASTM International: West Conshohocken, PA, USA, 2022.
11. *ASTM C563-16*; Standard Guide for Approximation of Optimum SO3 in Hydraulic Cement Using Compressive Strength. ASTM International: West Conshohocken, PA, USA, 2016.
12. Khudyakova, T.M.; Kolesnikova, O.G.; Zhanikulov, N.N.; Botabaev, N.E.; Kenzhibaeva, G.S.; Iztleuov, G.M.; Suigenbaeva, A.Z.; Kutzhanova, A.N.; Ashirbaev, H.A.; Kolesnikova, V.A. Low-Basicity Cement, Problems and Advantages of its Utilization. *Refract. Ind. Ceram.* **2021**, *62*, 369–374. [CrossRef]
13. Kolesnikova, O.; Vasilyeva, N.; Kolesnikov, A.; Zolkin, A. Optimization of raw mix using technogenic waste to produce cement clinker. *Mining Inf. Anal. Bull.* **2022**, *10–11*, 103–115. [CrossRef]
14. Lerch, W. The Influence of Gypsum on the Hydration and Properties of Portland Cement Pastes. *Proc. Am. Soc. Test. Mater.* **1946**, *46*, 1252–1291.
15. Fincan, M. Sulfate Optimization in the Cement-Slag Blended System Based on Calorimetry and Strength Studies. Ph.D. Thesis, University of South Florida, Tampa, FL, USA, 2021; p. 2. Available online: https://digitalcommons.usf.edu/cgi/viewcontent.cgi?article=9967&context=etd (accessed on 7 April 2023).
16. Bentur, A. Effect of Gypsum on the Hydration and Strength of C3S Pastes. *J. Am. Ceram. Soc.* **1976**, *59*, 210–213. [CrossRef]
17. Jelenić, I.; Panović, A.; Halle, R.; Gaćeša, T. Effect of gypsum on the hydration and strength development of commercial portland cements containing alkali sulfates. *Cem. Concr. Res.* **1977**, *7*, 239–245. [CrossRef]
18. Soroka, I.; Abayneh, M. Effect of gypsum on properties and internal structure of PC paste. *Cem. Concr. Res.* **1986**, *16*, 495–504. [CrossRef]
19. Sersale, R.; Cioffi, R.; Frigione, G.; Zenone, F. Relationship between gypsum content, porosity and strength in cement. I. Effect of SO3 on the physical microstructure of Portland cement mortars. *Cem. Concr. Res.* **1991**, *21*, 120–126. [CrossRef]

20. Tennis, P.D.; Jennigs, H.M. A model for two types of calcium silicate hydrate in the microstructure of Portland cement pastes. *Cem. Concr. Res.* **2000**, *30*, 855–863. [CrossRef]

21. Jansen, D.; Goetz-Neunhoeffer, F.; Stabler, C.; Neubauer, J. A remastered external standard method applied to the quantification of early OPC hydration. *Cem. Concr. Res.* **2011**, *41*, 602–608. [CrossRef]

22. Gunay, S.A.A. Influence of Aluminates Phases Hydration in Presence of Calcium Sulfate on Silicates Phases Hydration: Consequences on Cement Optimum Sulfate. Ph.D. Thesis, University of Bourgogne, Bourgogne, France, 2012. Available online: https://theses.hal.science/tel-00767768 (accessed on 7 April 2023).

23. Termkhajornkit, P.; Vu, Q.H.; Barbarulo, R.; Daronnat, S.; Chanvillard, G. Dependence of compressive strength on phase assemblage in cement pastes: Beyond gel–space ratio—Experimental evidence and micromechanical modeling. *Cem. Concr. Res.* **2014**, *56*, 1–11. [CrossRef]

24. Zunino, F.; Scrivener, K. The influence of sulfate addition on hydration kinetics and C-S-H morphology of C_3S and C_3S/C_3A systems. *Cem. Concr. Res.* **2022**, *160*, 106930. [CrossRef]

25. Andrade Neto, J.S.; de Matos, P.R.; De la Torre, A.G.; Campos, C.E.M.; Torres, S.M.; Monteiro, P.J.M.; Kirchheim, A.P. Hydration and interactions between pure and doped C_3S and C_3A in the presence of different calcium sulfates. *Cem. Concr. Res.* **2022**, *159*, 106893. [CrossRef]

26. Miller, F.M.; Tang, F.J. The distribution of sulfur in present-day clinkers of variable sulfur content. *Cem. Concr. Res.* **1996**, *26*, 1821–1829. [CrossRef]

27. Taylor, H.F.W. Distribution of sulfate between phases in Portland cement clinkers. *Cem. Concr. Res.* **1999**, *29*, 1173–1179. [CrossRef]

28. Horkoss, S.; Lteif, R.; Rizk, T. Influence of the clinker SO_3 on the cement characteristics. *Cem. Concr. Res.* **2011**, *41*, 913–919. [CrossRef]

29. Mohammed, S.; Safiullah, O. Optimization of the SO_3 content of an Algerian Portland cement: Study on the effect of various amounts of gypsum on cement properties. *Constr. Build. Mater.* **2018**, *164*, 262–370. [CrossRef]

30. Yamashita, H.; Yamada, K.; Hirao, H.; Hoshino, S. Influence of Limestone Powder on the Optimum Gypsum Content for Portland Cement with Different Alumina Content. Available online: https://www.researchgate.net/publication/285554157_Influence_of_Limestone_Powder_on_the_Optimum_Gypsum_Content_for_Portland_Cement_with_Different_Alumina_Content (accessed on 7 April 2023).

31. Irassar, E.F.; Violini, D.; Rahhal, V.F.; Milanesi, C.; Trezza, M.A.; Bonavetti, V.L. Influence of limestone content, gypsum content and fineness on early age properties of Portland limestone cement produced by inter-grinding. *Cem. Concr. Compos.* **2011**, *33*, 192–200. [CrossRef]

32. Liu, F.; Lan, M.Z. Effects of Gypsum on Cementitious Systems with Different Mineral Mixtures. Available online: https://www.researchgate.net/publication/269647645_Effects_of_Gypsum_on_Cementitious_Systems_with_Different_Mineral_Mixtures (accessed on 7 April 2023).

33. Adu-Amankwah, S.; Black, L.; Skocek, J.; Ben Haha, M.; Zajac, M. Effect of sulfate additions on hydration and performance of ternary slag-limestone composite cements. *Constr. Build. Mater.* **2018**, *164*, 451–462. [CrossRef]

34. Han, F.; Zhou, Y.; Zhang, Z. Effect of gypsum on the properties of composite binder containing high- volume slag and iron tailing powder. *Constr. Build. Mater.* **2020**, *252*, 119023. [CrossRef]

35. Tsamatsoulis, D.; Nikolakakos, N. Optimizing the Sulphates Content of Cement Using Multivariable Modelling and Uncertainty Analysis. *Chem. Biochem. Eng. Q.* **2013**, *27*, 133–144. Available online: http://silverstripe.fkit.hr/cabeq/assets/Uploads/Cabeq-2013-02-03.pdf (accessed on 19 June 2023).

36. Al Salaheen, M.; Alaloul, W.S.; Malkawi, A.B.; de Brito, J.; Alzubi, K.M.; Al-Sabaeei, A.M.; Alnarabiji, M.S. Modelling and Optimization for Mortar Compressive Strength Incorporating Heat-Treated Fly Oil Shale Ash as an Effective Supplementary Cementitious Material Using Response. *Materials* **2022**, *15*, 6538. [CrossRef]

37. Magistri, M.; Lo Presti, A.; Salvioni, D. Limestone and Fly Ash Blended Cements: Correlation between Durability, Performances and Particle Size Distribution. Available online: http://civmin.utoronto.ca/wp-content/uploads/2019/05/28.pdf (accessed on 7 April 2023).

38. Hirch, T.; Lu, Z.; Stepan, D. Impact of triethanolamine on the sulfate balance of Portland cements with mixed sulfate carriers. *J. Am. Ceram. Soc.* **2021**, *104*, 4829–4842. [CrossRef]

39. Recchi, P.; Magistri, M.; Lo Presti, A.; Cerulli, T. Influences of the Type and Amount of Calcium Sulphate on the Reactivity of Alkanolamine-Based Set Accelerators/Strength Improvers. Available online: http://cadd.mapei.com/wp-content/uploads/2011/07/2011-07-ICCC-Recchi-et-al_influence-of-calcium-sulphates.pdf (accessed on 7 April 2023).

40. Andrade Neto, J.S.; De la Torre, A.G.; Kirchheim, A.P. Effects of sulfates on the hydration of Portland cement—A review. *Constr. Build. Mater.* **2021**, *279*, 122428. [CrossRef]

41. Schade, T.; Middendorf, B. Use of Design of Experiments (DoE) to Model the Sulphate Agent Amount of (Ultra) Finely Ground and Fast Hardening Portland Cement Clinker. *Materials* **2021**, *14*, 5573. [CrossRef]

42. Kurdowski, W. *Cement and Concrete Chemistry*; Springer Science & Business Media: New York, NY, USA, 2014; pp. 217–218.

43. Escobar, C.A.; Morales-Menendez, R. Process-Monitoring-for-Quality—A Model Selection Criterion for Shallow Neural Networks. Available online: https://www.academia.edu/86483788/Process_monitoring_for_quality_A_model_selection_criterion (accessed on 7 April 2023).

44. Tsamatsoulis, D. Prediction of Cement Compressive Strength by Combining Dynamic Models of Neural Networks. *Chem. Biochem. Eng. Q.* **2021**, *35*, 295–318. [CrossRef]

45. *CEN/TC 51, EN 196-1:2016*; Methods of Testing Cement—Part 1: Determination of Strength. CEN Management Centre: Brussels, Belgium, 2016.

46. Tsamatsoulis, D. Simulation of Cement Grinding Process for Optimal Control of SO$_3$ Content. *Chem. Biochem. Eng. Q.* **2014**, *28*, 13–25. Available online: https://hrcak.srce.hr/en/clanak/174265 (accessed on 19 June 2023).

47. *CEN/TC 51, EN 196-6:2010*; Methods of Testing Cement—Part 6: Determination of Fineness. CEN Management Centre: Brussels, Belgium, 2010.

48. *CEN/TC 51, EN 196-2:2013*; Methods of Testing Cement—Part 2: Chemical Analysis of Cement. CEN Management Centre: Brussels, Belgium, 2013.

49. Pritzel, C.; Emami, M.; Afflerbach, S.; Killian, M.; Trettin, R. Formation of α-Hemihydrate Inside of a Gypsum Crystal during the Dehydration Process. *Crystals* **2022**, *12*, 1780. [CrossRef]

50. Krause, F.; Renner, B.; Coppens, F.; Dewanckele, J.; Schwotzer, M. Reactivity of Gypsum-Based Materials Subjected to Thermal Load: Investigation of Reaction Mechanisms. *Materials* **2020**, *13*, 1427. [CrossRef]

51. Tang, F.J.; Gartner, E.M. Influence of sulfate source on Portland cement hydration. *Adv. Cem. Res.* **1988**, *1*, 67–74. [CrossRef]

52. Staněk, T.; Sulovský, P. The influence of the alite polymorphism on the strength of the Portland cement. *Cem. Concr. Res.* **2002**, *32*, 1169–1175. [CrossRef]

53. Celic, I.B. The effects of particle size distribution and surface area upon cement strength development. *Powder Technol.* **2009**, *188*, 272–276. [CrossRef]

54. Rapid Laboratory Particle Size Analysis of Cements Using Laser Diffraction. Available online: https://www.bettersizeinstruments.com/uploads/file/rapid-laboratory-particle-size-analysis-of-cements-using-laser-diffraction.pdf (accessed on 7 April 2023).